Copyright Warning & Restrictions

The copyright law of the United States (Title 17, United States Code) governs the making of photocopies or other reproductions of copyrighted material.

Under certain conditions specified in the law, libraries and archives are authorized to furnish a photocopy or other reproduction. One of these specified conditions is that the photocopy or reproduction is not to be "used for any purpose other than private study, scholarship, or research." If a, user makes a request for, or later uses, a photocopy or reproduction for purposes in excess of "fair use" that user may be liable for copyright infringement,

This institution reserves the right to refuse to accept a copying order if, in its judgment, fulfillment of the order would involve violation of copyright law.

Please Note: The author retains the copyright while the New Jersey Institute of Technology reserves the right to distribute this thesis or dissertation

Printing note: If you do not wish to print this page, then select "Pages from: first page # to: last page #" on the print dialog screen

ABSTRACT

MAGNETIC AUGMENTED ROTATION SYSTEM (MARS) - PROPERTIES AND PERFORMANCE

by
Ruolei Liu

Magnetic Augmented Rotation System (MARS) is proposed as a system for conversion of mechanical energy into electrical energy. It works on the principle of magnetic coupling. Because it is contactless, compared with traditional gears, it increases the transfer efficiency from a driver to a rotor; reduces noise, requires no lubrication and has low maintenance cost. In order to assess the performance of MARS, a charging system based on MARS is implemented. This system includes rechargeable batteries in the range of 6 volts to 12 volts, a load in the form of a light bulb, a voltage transformer, and digital multimeter to monitor current/voltage in real-time. Additionally, infrared imaging is utilized during charging the rechargeable battery to monitor changes in temperature.

MAGNETIC AUGMENTED ROTATION SYSTEM (MARS) - PROPERTIES AND PERFORMANCE

by
Ruolei Liu

A Thesis
Submitted to the Faculty of
New Jersey Institute of Technology
in Partial Fulfillment of the Requirements for the Degree of
Master of Science in Materials Science and Engineering

Interdisciplinary Program in Materials Science and Engineering

May 2016

APPROVAL PAGE

MAGNETIC AUGMENTED ROTATION SYSTEM (MARS)
- PROPERTIES AND PERFORMANCE

Ruolei Liu

Dr. Nuggehalli M. Ravindra, Thesis Advisor — Date
Professor, Department of Physics, NJIT
Director, Interdisciplinary Program in Materials Science and Engineering, NJIT

Dr. Michael Jaffe, Committee Member — Date
Research Professor, Department of Biomedical Engineering, NJIT

Dr. Eon Soo Lee, Committee Member — Date
Assistant Professor, Mechanical and Industrial Engineering, NJIT

BIOGRAPHICAL SKETCH

Author: Ruolei Liu

Degree: Master of Science

Date: May 2016

Undergraduate and Graduate Education:

- Master of Science in Materials Science and Engineering, New Jersey Institute of Technology, Newark, NJ, 2016
- Bachelor of Science in Materials Science and Engineering, Xi'an Jiaotong University, Shaanxi, China, 2014

Major: Materials Science and Engineering

< To Yan’an Liu and Lijing Zhu, my dearest parents >

亲爱的爸爸妈妈，永远爱你们

ACKNOWLEDGMENT

I really want to extend my deepest appreciation to those who supported me and guided me all this time; you light up my life and leave behind wonderful memories of mine. These memorable two years is a treasure for my future. Here, I feel honored to have the opportunity to appreciate the following people who made my life gorgeous.

Firstly, I want to sincerely thank N.M. Ravindra, my thesis advisor, for all the advice and support he offered me. He gave me continuous advice and hints on my studies. He treated me always as his family and gave me love and encouragement, which made me feel like home even though actually I am thousands of miles away. Also, I want to convey my sincere gratitude to Tien-See Chow. I genuinely appreciate his help.

Secondly, I want to render sincere appreciation to my thesis committee members: Dr. Michael Jaffe and Dr. Eon Soo Lee. They offered timely help and penetrating suggestions for the improvement of my thesis.

Additionally, I want to express my warmest thanks to my team member, Shuang Du. I appreciate the immense cooperation and collaboration with Shuang.

Lastly, I want to express the deepest love to my friends, Yiliang, Lin, Chenyuan, Kaiqiang and Dinghao. Our friendship will last forever.

The partial financial support of Professor N.M. Ravindra and Mr. Tiensee Chow is acknowledged with thanks.

TABLE OF CONTENTS

TABLE OF CONTENTS
(Continued)

Chapter **Page**

TABLE OF CONTENTS
(Continued)

Chapter **Page**

LIST OF TABLES

LIST OF TABLES
(Continued)

LIST OF FIGURES

LIST OF FIGURES
(Continued)

LIST OF CHARTS

CHAPTER 1

INTRODUCTION

Magnetic Augmented Rotation System (MARS) facilitates in the conversion of mechanical energy into electrical energy and works by contactless magnetic coupling. Compared with traditional mechanical gears, MARS offers increased conversion efficiency, reduces noise and maintenance costs. MARS has significant potential in various sectors of the industry. Therefore, the analyses of the properties of MARS and the knowledge of its performance are of great importance.

In Chapter 1, a brief introduction to the structure of the thesis is presented. Chapter 2 introduces the fundamentals of magnetic materials. In Chapter 3, more details of MARS are described. Chapter 4 describes the characteristics of MARS, and a charging system based on MARS is developed. The test results of MARS and the charging system is analyzed in Chapter 5. 4 AAA batteries, each of which has rated voltage of 1.5V, will be charged for desired duration by utilizing the MARS system. Additionally, the infrared image of the system during charging is taken. In Chapter 6, the test results and the MARS charging system is further analyzed.

CHAPTER 2

FUNDAMENTALS OF MAGNETIC MATERIALS

In recent years, magnetic materials have been widely developed and used in many areas. In order to have a better understanding of its properties, this chapter will introduce some basic knowledge of magnetic materials, such as the history, magnetic field, magnetic moment and magnetic energy. Also, several typical magnetic materials will be introduced. In the last part of this chapter, some applications of magnetic materials in industry and in our daily lives will be summarized.

2.1 Historical Background

In 600 B.C., people found a form of a mineral. From then on, people made use of its ability to attract other pieces of the same material and iron for a thousand years. However, only in modern times that the scientists began to understand it, and develop technologies based on this understanding.

Danish physicist Hans Christian Oersted first suggested a link between electricity and magnetism, which is a great contribution to electromagnetism. In 1822, Ampère explained magnetic materials based on a small circular electric current, which is the first explanation of a molecular magnet. Moreover, Ampère's circuital law points out that the concept of magnetic dipoles is similar to electric dipoles. In Figure 2.1, a schematic of the macroscopic electromagnetic phenomena is presented. From this figure, we can see that a bar magnet and a circuital current in a wire are physically equivalent. Even though

scientists had performed extensive research on magnetism, its origin was still not totally understood until the finding of quantum mechanics.

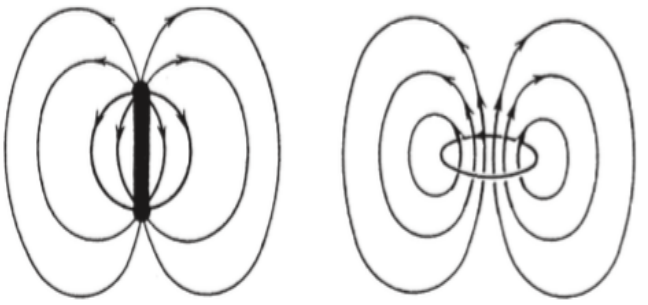

Figure 2.1 Magnetic fields due to a bar magnet and a circuital current.

Source: Gertz I. Likhtenshtein, Jun Yamauchi, Shin'ichi Nakatsuji, Alex I. Smirnov, Rui Tamura (2008) Nitroxides: Applications in Chemistry, Biomedicine, and Materials Science.

Before the birth of quantum mechanics, numerous experiments and data of the magnetic properties of materials were accumulated, and observing the response of every material to a magnetic field is one of them. Gouy and Faraday invented these experiments by using magnetic balance. The principle of measurement is shown in Figure 2.2; the measured force is equal to the force exerted on the material in a magnetic field. Depending on the direction of the force, materials can be divided into two types, diamagnetic and paramagnetic. The difference between these two is caused by the absence or presence of the magnetic moments that some materials possess in atoms, ions, or molecules.

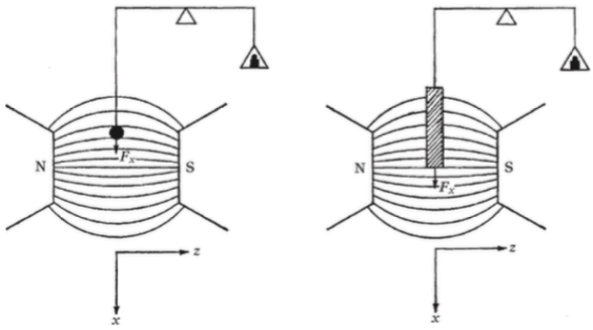

Figure 2.2 Faraday and Gouy balances for magnetic measurements. Force (Fx) is measured.

Source: Gertz I. Likhtenshtein, Jun Yamauchi, Shin'ichi Nakatsuji, Alex I. Smirnov, Rui Tamura (2008) Nitroxides: Applications in Chemistry, Biomedicine, and Materials Science.

The modern understanding of magnetic phenomena in condensed matter originates from the work of Curie and Weiss. Curie discovered that the magnetic coefficients of attraction of paramagnetic bodies vary in inverse proportion to the absolute temperature—Curie's law. Weiss proposed a theory of magnetism based on an internal molecular field proportional to the average magnetization that spontaneously align the electronic micromagnets in magnetic matter [1].

2.2 Magnetic Field

Magnetic field is similar to gravitational fields, because both of them cannot be seen and touched. The difference is that we can feel the power of the Earth's gravitational fields ourselves without any other help. But we do not experience magnetic fields in such a direct way. Actually, the existence of magnetic field can only be seen due to its effect on objects, such as magnetized pieces of metal, loadstone, or copper coil that carry an electrical current. For example, if we place a magnetized needle in a magnetic field, it

will slowly align itself with the field. When we turn on the current in a copper wire, we can see that the compass needle jumps abruptly. All these phenomena led to the development of the concept of magnetic fields.

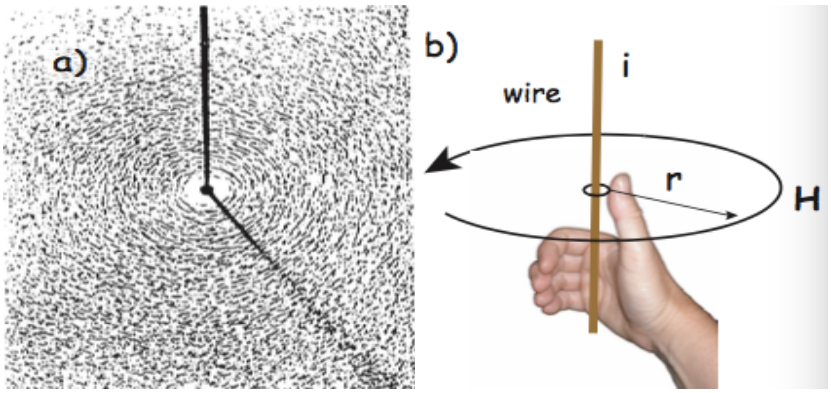

Figure 2.3 a) Distribution of iron filings on a flat sheet pierced by a wire carrying a current i. b) Relationship of magnetic field to current for straight wire.

Source: The physics of magnetism, Magnetic information consortium, https://earthref.org/MagIC/books/Tauxe/Essentials/WebBook3ch1.html

Since electric current generates magnetic fields, we can define the magnetic field in terms of the electric current that creates it. In Figure 2.3(a), we can clearly see what happens when a flat sheet with a wire carrying a current i. As seen in the picture, the iron filings on the sheet will line up with the magnetic field, which is produced by the current in the wire. Figure 2.3(b) illustrates the right-hand rule. That is, when the right thumb points in the direction of current flow, the fingers will curl in the direction of the magnetic field. The magnitude of H is proportional to the strength of the current i. According to Ampère's circuital law, H can be express as:

$$H = \frac{i}{2\pi r} \tag{2.1}$$

where r is the length of the vector r. So we can infer that the unit of H is Am^{-1}.

In many expressions, we can also find that B represents the magnetic field. Actually B and H are closely related, but not the same. Strictly speaking, B is the induction and H is the field, even though the distinction is often blurred. The relationship between these two is given by:

$$B = \mu(H + M) \tag{2.2}$$

where μ is a physical constant known as the permeability. M is the magnetization of the material. The permeability for free space in vacuum is μ_0, $= 4\pi \times 10^{-7} H \cdot m^{-1}$.

2.3 Magnetic Moment

The electric current in a wire produces a magnetic field that goes around the wire.

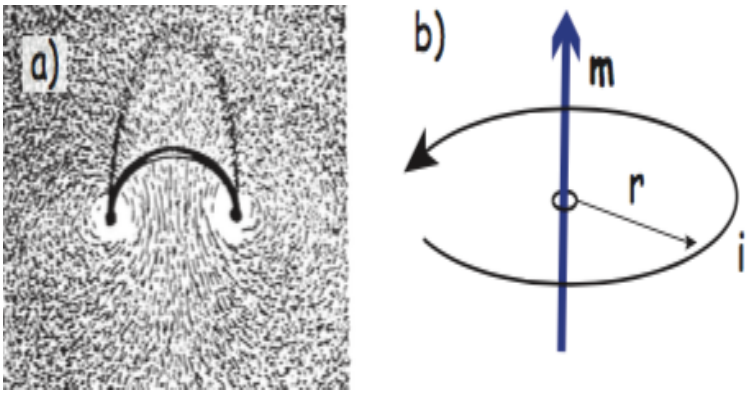

Figure 2.4 a) Iron filings show the magnetic field generated by current flowing in a loop. b) A current loop with current i and area πr^2 produces a magnetic moment m.

Source: The physics of magnetism, Magnetic information consortium, https://earthref.org/MagIC/books/Tauxe/Essentials/WebBook3ch1.html

As shown in Figure 2.4, if we bend the wire into a loop with an area πr^2, which carries a current i, the created magnetic field is shown by the pattern of the iron filings. So, we can calculate the magnitude of the hypothetical magnet in terms of a magnetic moment m. The magnetic moment is created by a current i and also depends on the area of the current loop. It can be quantified by:

$$m = i\pi r^2 \tag{2.3}$$

Also, the unit of m is Am^2.

2.4 Magnetic Energy

A magnetic moment m in a magnetic field B has magnetostatic energy, E_m. This energy tends to align compass needles with the magnetic field. E_m given by:

$$E_m = -mB\cos\theta \tag{2.4}$$

where m and B are the magnitude of magnetic moment and magnetic field, respectively. θ is the angle between them.

2.5 Magnetic Materials

According to their behavior, magnetic materials can be classified as diamagnetic materials, paramagnetic materials, ferromagnetic materials, ferrimagnetic materials and antiferromagnetic materials.

2.5.1 Diamagnetic Materials

Diamagnetism is a quantum mechanical effect that occurs in all materials. So to a different degree, it is a property of all materials and will make a contribution when the material is placed in a magnetic field. However, the material can be called a diamagnet when diamagnetism is the only contribution. For some other materials, the diamagnetic contribution becomes negligible. Actually, diamagnet is not a permanent magnet. As shown in Figure 2.5 below, in the diamagnetic material, atoms have no magnetic moment when there is no applied field. The electrons will spin under the influence of an applied field (H), which also produces a magnetization (M) at the same time. The direction of the

magnetization is opposite to that of the applied field.

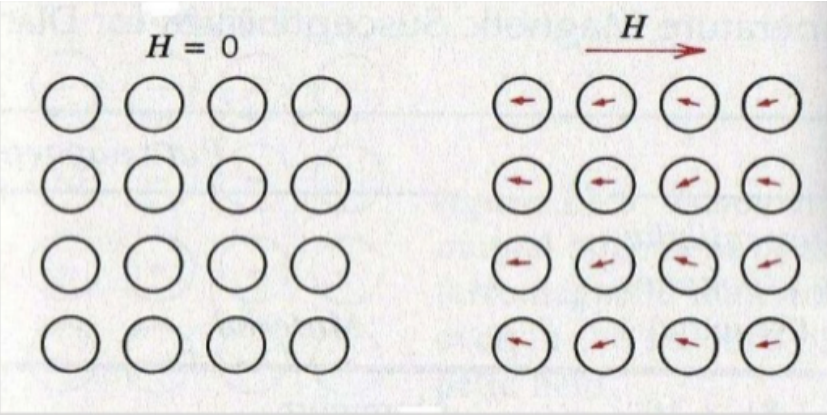

Figure 2.5 Diamagnetism.

Source: DivYesh Patel(2015) Diamagnetism,paramagnetism,ferromagnetism,antiferromagnetism and ferrimagnetism

2.5.2 Paramagnetic Materials

Paramagnetic materials have a small, positive susceptibility to magnetic field. When a magnetic field is applied, they are slightly attracted and do not retain the magnetic properties when the field is removed. This is because the thermal motion caused by the applied field randomizes the spin orientations. When the applied field is removed, the total magnetization will drop to zero. Only a small fraction of spins will orient in the presence of the magnetic field. Paramagnetic materials include magnesium, molybdenum, tantalum, and lithium.

2.5.3 Ferromagnetic Materials

Compared to all other types of magnetism, ferromagnetism is the strongest one. This is because, in ferromagnetic materials, the atoms are arranged in a lattice and the atomic magnetic moments interact to align parallel to each other. This effect is explained in

classical theory by the presence of a molecular field within the ferromagnetic material, which was first postulated by Weiss in 1907 [2]. This field can magnetize the material to saturation. Further, Heisenberg proposed that there are parallel alignments of magnetic moments in ferromagnetic materials, and these moments can exchange between neighboring moments. Weiss postulated that domains are present in these aligned magnetic moments. When a magnetic field is applied, the response of these domains determine the overall properties of the material. At and above room temperature, only Fe, Co and Ni are ferromagnetic materials. When the material is heated, the atoms are activated and the degrees of alignment for magnetic moments decrease; hence, the saturation magnetization decreases.

2.5.4 Antiferromagnetic Materials

Unlike in ferromagnetic materials, the magnetic moments in antiferromagnetic materials are aligned antiparallel, as a result of the exchange interaction between neighboring atoms. Therefore, the magnetic field cancels out when magnetic field is applied. However, they have transition temperature like ferromagnetic materials, which is known as Néel temperature.

2.5.5 Ferrimagnetic Material

Ferrimagnetism is only observed in compounds, which have more complex crystal structures than pure elements. The exchange interactions within these materials lead to parallel alignment of atoms in some crystal site and antiparallel alignment in others. Like a ferromagnetic material, ferrimagnetic material is made up of magnetic domains; the difference is that the domains are not in the same direction with applied magnetic field, so the saturation is lower for an applied magnetic field.

2.6 Applications of Magnetic Materials

Magnetic materials are divided into two categories, soft magnets and hard magnets, depending on the difficulty of demagnetization. For hard magnets, they tend to remain magnetized for a period of time. They are difficult to demagnetize unless a certain magnetic field, which depends on the coercivity, is applied. In contrast, soft magnets can be magnetized and will lose magnetization over time. Therefore, since soft magnets have small remanence and small coercivity, such as silicon steel, nickel steel and ferrites, they are the best choice for devices working in alternating magnetic fields. For example, the core inside solenoid is made of soft magnets.

An electromagnet is a type of magnet in which the magnetic field is produced by an electric current. This magnetic field will disappear when the current is turned off. To concentrate the magnetic flux and make it more powerful, the electromagnets usually consist of a large number of closed spaced wires, which are made from ferromagnetic or ferrimagetic material such as iron. Compared to the permanent magnet, the main advantage of the electromagnet is that the magnetic field is easy to be controlled by changing the amount of electric current in the winding. On the other hand, the disadvantage is that the electromagnet requires a continuous supply of current to maintain the magnetic field. Electromagnets can be used in many devices such as motors, generators, relays, Magnetic resonance Imaging (MRI) machines etc. They can also be employed to move heavy iron-containing objects such as steel [3].

A ferrite is a type of ceramic compound composed of iron oxide (Fe_2O_3) combined chemically with one or more additional metallic elements [4]. Actually, ferrites can be divided into two types depending on their coercivity: hard ferrites and soft ferrites.

For hard ferrites, they have high coercivity and are difficult to demagnetize. They are used in devices such loudspeakers, refrigerator magnets and small electric motors. Early computer memories stored data in the residual magnetic field of hard ferrite cores. For soft ferrites, their coercivity is low. They are used in the electronics industry to make ferrite cores for inductors and transformers, and in various microwave components. Yogoro Kato and Takeshi Takei of the Tokyo Institute of Technology invented this material in 1930 [5].

Magnetic tape, made of a thin magnetizable coating on a long and narrow strip of plastic film, is used for recording. The tape head on magnetic tape can magnetically manipulate the surface of the oxide side, by which the information is stored. The other side is just a substrate to hold the tape tighter. The magnetic side of most tapes is made of an oxide of iron, sometime chromium. Magnetic tapes are widely used in recording. They allow the different recording to be mixed and edited with tolerable loss in quality. It is also a key technology in early computer development. In magnetic tapes, unparalleled amount of data can be created and stored, and to be easily accessed.

Some hard magnetic materials, like ferrites, NdFeB (neodymium-iron-boron) and SmCo (samarium-cobalt) are also used as sensors by providing a bias field in the sensor assembly. This bias field interacts with the object being sensed and a sensor element detects the changes in the bias fields caused by this interaction. Figure 2.6 shows a simple ferrous article proximity detector made in this way. The flux measured at the pole face of the bias magnet varies inversely with the distance of the target from the pole face.

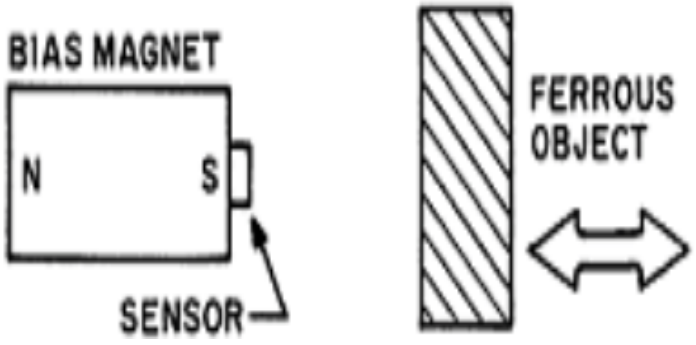

Figure 2.6 A simple proximity sensor can be made to detect ferrous objects by measuring changes in a bias field caused by the presence of the target.

Source: Ed Ramsden (1998) Electric/Magnetic Sensor Applications for Magnetic Materials

CHAPTER 3

DESCRIPTION OF MAGNETIC AUGMENTED ROTATION SYSTEM (MARS)

In order to have a better understanding of Magnetic Augmented Rotation System (MARS), in this chapter, some basic knowledge of magnetic gears will be introduced. Then MARS, which can be implemented as magnetic gears, will be described. Further, some modifications of MARS and its advantages by comparing with common magnetic gear will be presented.

3.1 Magnetic Gears

3.1.1 History and Development

The idea of magnetic gears (MG) was first introduced in the beginning of 20th century. In 1913, a US Patent [6] described an electromagnetic gear, which was regarded as the first topology of electromagnetic gears. In this patent, the inventor provided a method of and apparatus for coupling two shafts or rotatable elements together without the employment of any mechanical or tangible means connecting said shafts. However，this novel idea did not draw any attention at that time. People started to pay attention to MG because of another US Patent by Faus [7] in 1941. Faus' magnetic gear has a geometric configuration analogous to ancient mechanical pin gears, with magnetic pins inserted in the base. Even though magnetic gears were more accepted at that time, the disadvantages still limited their application in industry. Since the gears were made by ferrite, the low mechanical and magnetic strength of ferrite seriously affected their performance and lifetime.

With the appearance of the high-performance neodymium iron boron (NdFeB) material in 1980s, the MGs aroused public attention again. A neodymium magnet is known to be the most commonly used type of rare-earth magnet, a permanent magnet made from an alloy of neodymium, iron and boron to form the $Nd_2Fe_{14}B$ tetragonal crystalline structure [8]. Nagrial et al. [9,10,11] made use of NdFeB magnets to allow an external-type magnetic gear set to generate high magnetic flux densities within the air gap. Being the strongest type of permanent magnet, NdFeB has replaced many other types of magnets in applications, especially in the area, which require strong permanent magnets.

Actually, the early MG topologies were derived from mechanical gear topologies. They simply replaced the slots and iron core teeth by N-poles and S-poles of PMs, respectively. So the poor torque density is still a key problem for the utilization of PMs.

3.1.2 Magnetic Gear System

Usually, the performance of an output magnetic gear mechanism is controlled by the megnetostatic field distribution; meanwhile, the magnetic field distribution of a magnetic gear mechanism is governed by its topological structure. In 1989, Tsurumoto [12] presented external and internal meshing magnetic gear sets with involute-curved magnets attached onto two overlapped mild-steel yokes. In 1991, Ikuta et al. [13] presented an external magnetic gear set and an internal magnetic gear set for use in microtransmission mechanisms. However, lacking the magnetic flux conducting system limits the transmitted torque capability and structural strength of the microtransmission mechanism, which restricted the application of this gear. In 1993, Kikuchi and Tsurumoto [14] proposed a magnetic worm and worm wheel with $SmCo_5$ magnets possessing a high-speed

reduction ratio of 1:33. In 1991, Mabe [15] patented a magnetic epicyclic gear train, which is analogous to a basic planetary gear train set, consisting of a magnetic sun gear, a magnetic planet gear, a carrier and a magnetic ring gear. The magnetic planet gear is close to the magnetic ring gear with an internal gear pair; at the same time, it is adjacent to the magnetic planet gear with an external gear pair. The carrier is located between the sun gear and the planet gear with revolute joints, which is used to maintain a constant center distance between the magnetic sun gear and the magnetic planet gear. Since the magnetic sun gear, carrier and the magnetic ring gear all rotate around the same central axis mounted on the frame, this connection mode is called coaxial links. In 1996, Yao et al. [16] proposed a bi-axial external magnetic gear set with sector-shaped permanent magnets. In Yao's prototype, he made some modifications compared to Ikuta's design in the magnetic flux system. A magnetic conductive back iron is employed on the rotor to provide the magnetic flux return paths. He found that the transmitted torque is sensitive to the yoke thickness, number of magnetic poles, magnetic material properties and the central distance of two magnetic gears [17]. Although several attempts have been made to improve the torque density, such as optimizing design parameters [18] and applying proper magnetic materials [19] to provide a stronger magnetic field, they are still far from satisfying the strict demands of industrial and transmitting applications. In 2001, Atallah and Howe proposed a high-performance MG named as the coaxial magnetic gear (CMG), whose principle of operation was based on the modulation of the magnetic fields produced by two PM rotors via the ferromagnetic pole-pieces [20,21]. Since all the PMs simultaneously contribute to torque transmission, CMG provides a higher torque density.

In brief, the coaxial magnetic gear (CMG) was made by three parts, inner rotor, outer rotor and steel pole-pieces. Permanent magnets are in both inner rotor and outer rotor; of course, their numbers are different. Since the steel pole-pieces are kept stationary, the outer rotor and the inner rotor rotate in different direction. The steel pole-pieces are very important because they can modulate the magnetic fields produced by the inner and outer permanent-magnet rotors. All permanent magnets are simultaneously operated for torque transmission; as a result, the transmitted torque density of such a coaxial topology is significantly improved. More information about CME are shown in Figure 3.1.

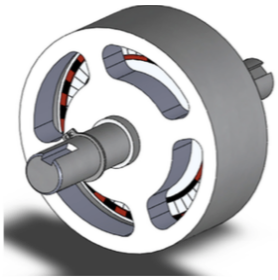

(a) An embodiment

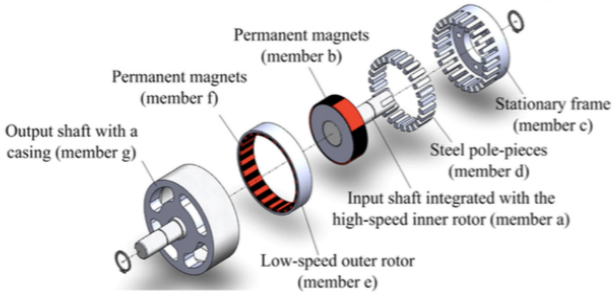

(b) Exploded view

Figure 3.1 A coaxial magnetic gear mechanism.

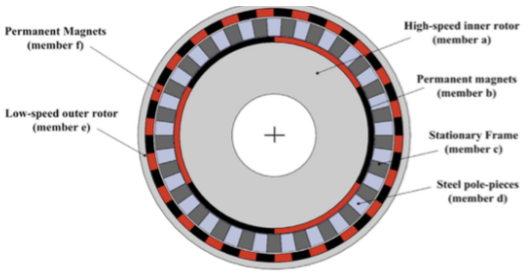

c) Cross sectional view

Figure 3.1 (Continued)A coaxial magnetic gear mechanism.

Source: Yi-Chang Wu, Bo-Syuan Jian (2013), Magnetic field analysis of a coaxial magnetic gear mechanism by two-dimensional equivalent magnetic circuit network method and finite-element method, International Applied Science and Precision Engineering Conference

Figure 3.1 (a) is an embodiment of a coaxial magnetic gear mechanism developed from Atallah's design [20]. The exploded view and the cross sectional view of the coaxial magnetic gear mechanism are explained in Figure 3.1 (b) and (c), respectively. As shown in Figure 3.1 (b), some permanent magnets (member b) are sited on the outer surface of the high-speed inner rotor (member a), while some permanent magnets (member f) are located in the inner surface of the low-speed outer rotor (member e). The output with a casing (member g) is affixed to the outer rotor. The stationary frame (member c), in which the steel pole-pieces (member d) are distributed evenly, are arranged in slots [22]. All of the stationary frame, the inner rotor and the output shaft with a casing are made of aluminum with low permeability. The steel pole-pieces and two rotor yokes are made of non-oriented silicon steel laminations to reduce the core loss. The inner rotor, the stationary frame and the low-speed outer rotor are separated by two air gaps between them. The modulation effect caused by the steel pole-pieces plays an important role in the transmission of torque, which allows the inner rotor to drive the outer rotor with a constant speed reduction. Suppose the numbers of the steel pole-pieces are n_s, the

numbers of the pole-pairs in the outer rotor are p_o, and the numbers of the pole-pairs in the inner rotor are p_i, the driving torque from the inner rotor to the outer rotor can be transmitted stable only when

$$n_s=p_i+p_o, \tag{3.1}$$

which means the ratio of the output shaft speed to the input shaft speed is $-\left({}^{p_i}/_{p_o}\right)$. The negative sign signifies opposite directions of the high-speed inner rotor and the low-speed outer rotor. For the coaxial magnetic gear mechanism shown in Figure 3.1, the numbers of the permanent magnets for the inner rotor and outer rotor are 3 and 22, respectively. So the total number of the steel pole-pieces is

$$3+22=25. \tag{3.2}$$

These steel pole-pieces are distributed evenly in the stationary frame to ensure that the field modulation effect is as expected. Thus, the speed reduction ratio of this mechanism is -3/22, which means the angular velocity of the inner rotor is 7.33 times that of the low-speed outer rotor, but in the opposite direction.

Magnetic planetary gear is another typical magnetic gear. As shown in Figure 3.2(a), the elementary planetary gear set has three different parts, a ring gear, a sun gear and four planet gears. The ring gear and the sun gear rotate around their own respective centers; however, the planet gears rotate around the unfixed centers and the center of the sun gear at the same time. Actually, there are three elementary types of

planetary gearbox commonly used in industry, which are shown in Figure 3.2(b)-(d). Planetary gearbox has some unique behaviors due to its unfixed-axis structure. For example, since the planet gears mesh with the sun gear and ring gear simultaneously, components like gears and bearing will vibrate similarly. The vibration with different phases couple with each other; as a result, some of the vibrations could be neutralized or cancelled.

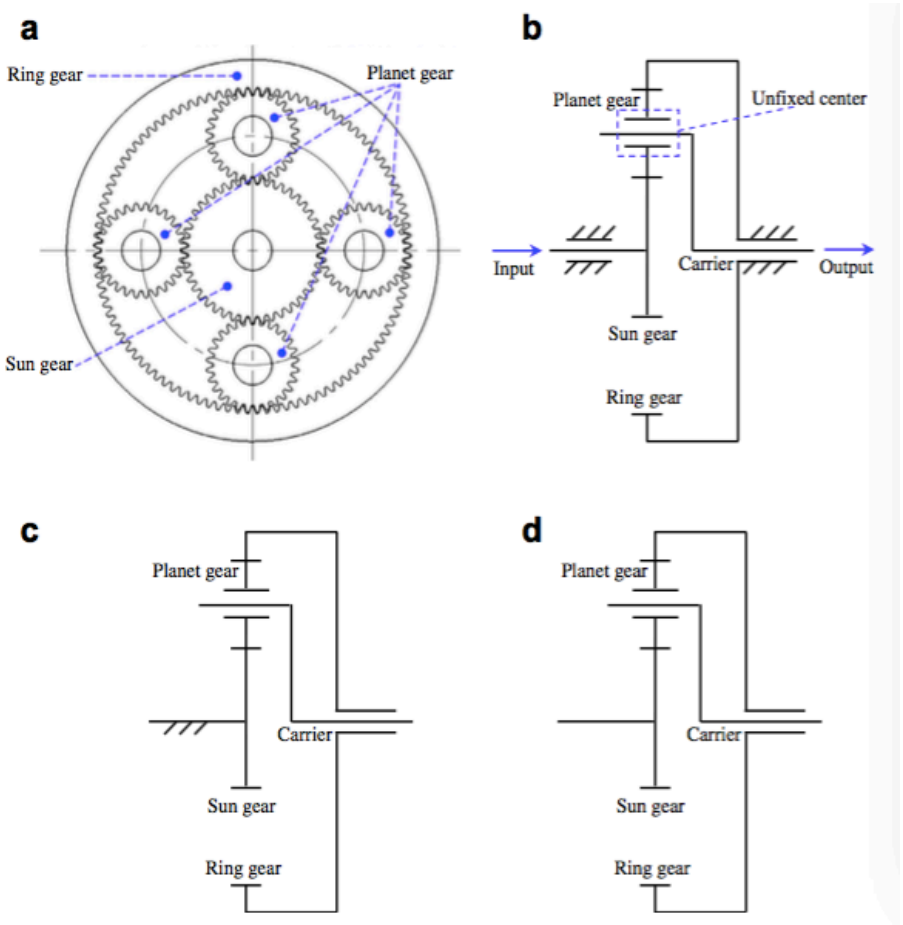

Figure 3.2 (a) An elementary planetary gear set having four planet gears, (b) scheme of planetary gear set with the standstill ring gear, (c) scheme of planetary gear set with the standstill sun gear and (d) scheme of planetary gearbox set with the rotating sun gear and the rotating ring gear.

Source: Yaguo Lei, Jing Lin, Ming J. Zuo (2014) Condition monitoring and fault diagnosis of planetary gearboxes: A review

3.1.3 Advantages

Compared to traditional mechanical gears, magnetic gears offer unique advantage; it saves maintenance needs and cost, and improves the efficiency, since the magnetic coupling between the input and output shafts is frictionless. Also, the gear will not be damaged when over-torque due to this non-contact characteristic; once the maximum transmitted torque has been exceeded, the gear just slightly slips. The connection between magnetic gears is also non-moving; thus, no friction is generated and no wear results during transmission of force and torque. They isolate the vibration as well; so much less acoustic noise is made, which overcomes the inherent disadvantages of the existing mechanical gears. All these advantages, such as no mechanical loss, inherent overload protection, high efficiency, make magnetic gear a better choice and has bright prospects in the future!

3.1.4 Applications of Magnetic Gear

As the research on magnetic gear goes deeper and deeper, we understand more about its characteristics, which offers an opportunity to make better use of magnetic gears in industry.

Wind power generation is a major way for utilizing wind power, which is an abundant, clear and renewable energy resource. There are two classifications in wind power generation, constant speed constant frequency (CSCF) and variable speed constant frequency (VSCF). For the VSCF system, several types of generators have been adopted. To be a generator, there are several requirements. Firstly, besides the mechanical gearbox, the generator is also driven by the wind turbine with its low-speed and high-torque operation. In another way, to be easily installed onto the tower, the battery system has to

be small size and lightweight. Usually, higher rotor speed implies lower electromagnetic torque, and electromagnetic torque is proportional to the volume of the machine. Hence, improving the rotor speed is a great way to reduce the volume of the machine, which means the weight of the machine is reduced at the same time. With the development of magnetic gear, it will gradually replace the traditional mechanical gear, especially the coaxial magnetic gear. The outer-rotor, which is low speed and high torque, can directly couple with turbine blades. Its relative larger diameter is convenient for accommodating multi-poles. At the same time, inner-rotor is high speed, which offers an opportunity to reduce the overall weight and size. The isolation between the input and output shafts provides some distinct advantages, too. For example, it is free from maintenance, offers precise peak torque transmission and has inherent overload protection.

The integrated in-wheel motor is also an application for magnetic gear. Being a core technology for electric vehicles, the high performance driving motor has to offer high-torque low-speed operation as well as lightweight. Mechanical gearboxes are engaged to match the high-speed motor and the relatively low-speed wheel. However, it has some problems due its contact mechanisms, such as transmission loss and noise. Certain magnetic gears can totally overcome these weaknesses, and they satisfy the low-speed requirement for direct driving and the high-speed requirement for motor design simultaneously. Moreover, the highly integrated design can dramatically reduce the overall size and weight.

3.2 Description of MARS

Magnetic Augment Rotation System, US Patent No.6356000 B1, was invented by Chun-Yuan Ho and Tien-See Chow. It was patented on Mar.12th, 2002. The aim of MARS is to improve the efficiency of the drive wheel and the prime mover. The whole system includes several parts: wheel assembly, first magnetic polarity, second magnetic polarity, bearing assembly, magnetic biasing assembly and anti-reversing gear assembly [23]. Like other magnetic gears, the power transform in MARS system from one wheel to another is by magnetic coupling rather than mechanical contacts. More details on MARS is shown in Figure 3.3.

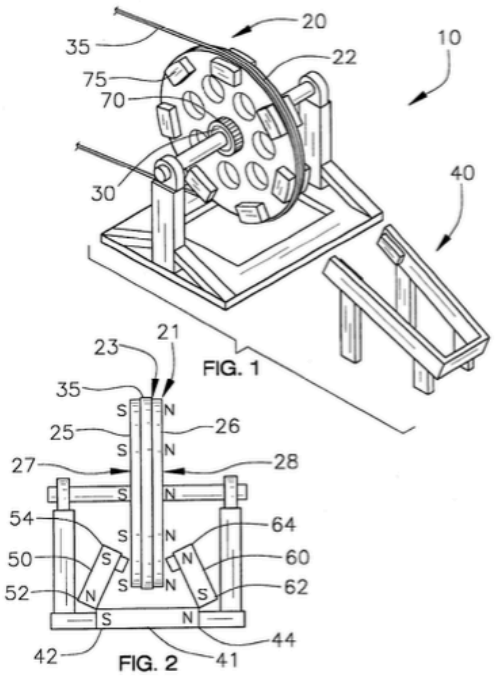

Figure 3.3 Schematic perspective views of MARS.

Source: Ho C-Y, Chow T-S (2002), Magnetically Augmented Rotation System, U.S. Patent 6356000 B1.

As illustrated in Figures 3.3 and 3.4, the Magnetic Augmented Rotation System 10 generally comprises a wheel assembly 20, a bearing assembly 30, a magnetic biasing assembly 40, and an anti-reversing gear assembly 70.

The wheel assembly 20 includes a central portion 22, a first magnetic assembly 25, and a second magnetic assembly 26. The second magnetic assembly 26 is a single magnetic disk coupled to the center portion 22. The surface 27 of the first magnetic assembly 25 has a first magnetic polarity, and the surface 28 of the second magnetic assembly 26 has the second polarity, opposite to the first one. The first magnetic assembly 25 and the second one 26 align with each other.

In the lower part of Figure 3.3, the magnets 75 are distributed uniformly in the first magnetic assembly 25 and the second magnetic assembly 26 at the same time. The two magnetic assemblies are aligned in the two side of the wheel assembly 20, asymmetrically.

An annular groove 23 is positioned around a circumference of the central portion 22 of the wheel assembly 20.

A drive belt 35, which is positioned in the annular groove 23, delivers the primary rotational force to the wheel assembly. This drive belt 35 may be a belt or a chain.

The magnetic biasing assembly 40 is made from three parts, the first linear magnet 41, the second linear magnet 50 and the third linear magnet 60. It can apply torque to the wheel assembly 20 by the interaction between the magnetic biasing assembly 40 and the two magnetic assemblies 25 and 26.

The first linear magnet 41 is positioned perpendicular with a plane, which extends from a focus of the wheel assembly 20. It is perpendicular to the surface 27 and 28, also.

The second linear magnet 50 is positioned next to one end 42 of the first magnet 41. There is an oblique angle between 50 and 25, to make sure that one side of 50 gets close to the first magnetic assembly 25 of the wheel assembly 20. The other end, 52 is placed next to one end 42 of the first magnet 41.

The third linear magnet 60 is placed adjacent to the other end of the first linear magnet 41, which is numbered 44. It is symmetrical to the second linear magnet 50 with the plane in which the wheel assembly 20 is in. This plane also passes through the midpoint of the linear magnet 41.

One end 42 of the first linear magnet 41 has North Pole, while the other end 44 has South Pole. The two ends of the second linear magnet 50, which is numbered 52 and 54, have the north and south poles, respectively; ends 64 and 62 of the third linear magnet 60 have north and south poles, respectively. One thing about the side of 50, 54, is very important that it has to have the same polarity with the magnets 75. In this way, these magnets with the same polarity offer a repelling force and help the wheel assembly 25 to drive easier. On one side 64 of the third linear magnet 60, it also causes a repelling force between the magnet 60 and the second magnetic assembly 26 according to corresponding polarities.

There is an anti-reversing gear assembly 70 connected to the wheel assembly 20, which prevents the MARS 10 to rotate reversely.

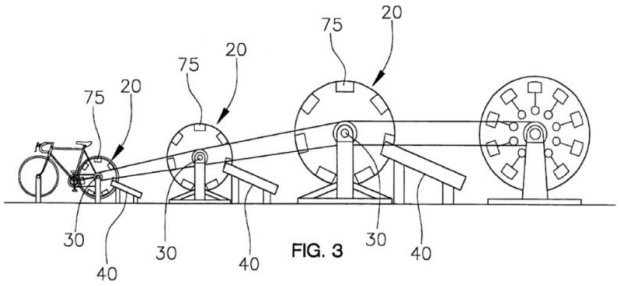

Figure 3.4 Schematic views of multiple embodiments of MARS in a cascade arrangement.

Source: Ho C-Y, Chow T-S (2002), Magnetically Augmented Rotation System, U.S. Patent 6356000 B1.

Figure 3.4 is a schematic view of multiple embodiments of the invention in a cascade arrangement. The bicycle on the left is the power input, and the plate on the right side is the load. The parts between these two are MARS with the same velocity. In this embodiment, the power generated by the driving system can be transmitted from the magnetic driver to the magnetic rotor by the magnetic coupling.

As a pollution-free instrument, MARS can be widely used in many fields, such as in electric vehicles, self-sustained wheel chairs, and small-scale wind turbines. Wind power, hydropower and hand-held power are all regarded as compatible power input to drive the MARS and the power output is scalable and controllable [24]. The electric charger on cars and trucks is usually 12 Volts or 24 Volts, which can be achieved by using MARS-based sustainable energy generation method. In this way, the traditional fossil fuel combustion for the direct-drive devices will be substituted, which reduce the use of energy and the pollution of air.

3.3 Improvement of MARS

Based on the original MARS system, several contactless gear systems has been designed and constructed.

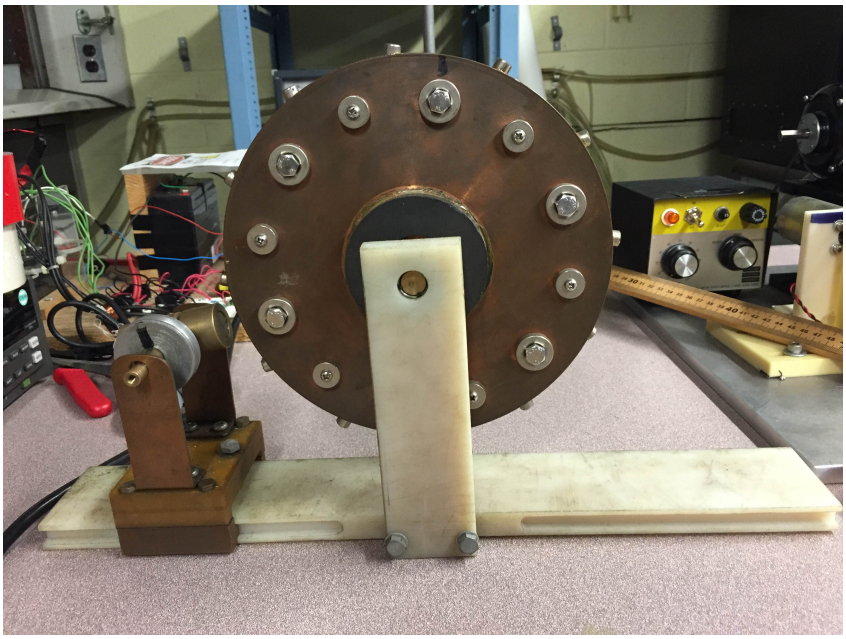

Figure 3.5 Prototype of MARS.

Figure 3.5 shows a prototype of MARS. The magnets are distributed uniformly in the wheel, with the same polarity towards outside. Next to the wheel, there is a cylindrical magnet, which has north polarity on one side and south polarity on the other side. When the cylindrical magnet is rotated, it will have the same polarity with the magnet on the wheel at some moment, which causes a repelling force between the cylider and the wheel. This repelling force will drive the wheel to rotate. Additionally, as the number of magnets on the wheel is enhanced and the magnetic field strengths are more concentrated, compared with the magnetic field strength of the cylindrical magnet, its rotation speed will increase.

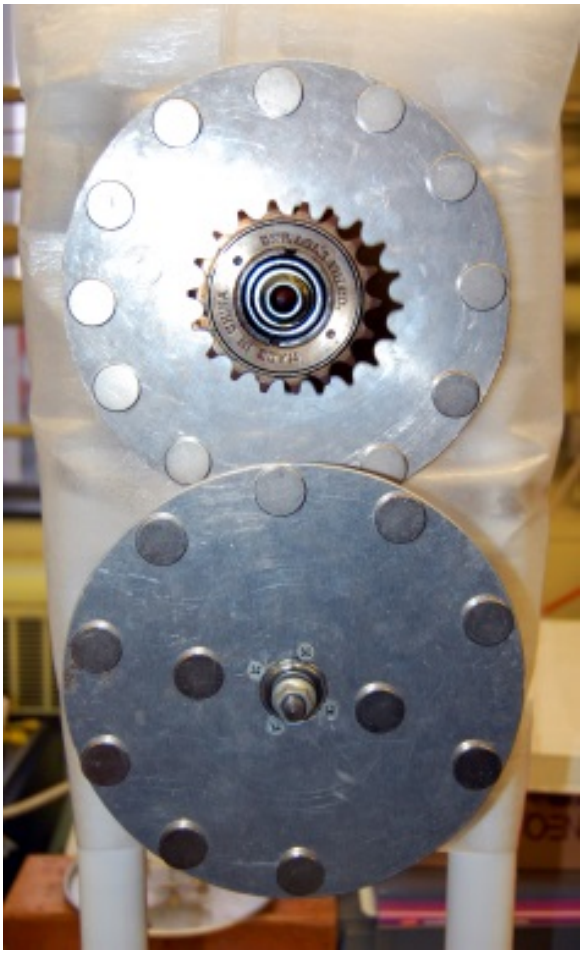

Figure 3.6 Contactless gear system.

In Figure 3.6, a set of small round rare earth magnets, in which opposite poles attract each other, are implemented on each of the two aluminum plates. To make these two wheels have magnetic repulsive force, the magnets in the outward of top wheel must have the same magnetic polarity with that in the inward of the bottom wheel. These magnets are distributed uniformly, in order that the transmission of torque and energy between the two wheels are smooth.

Actually, both of these two wheels can act as the driver; therefore, when the power is input into one of the wheels, the other one will move as the output wheel. Also, when torque is applied, these two wheels will rotate in the direction that is determined

primarily by the nature of the magnetic fields – i.e. force of attraction or repulsion. For example, in case of magnetic repulsive forces, if the top wheel is applied clockwise torque as power input, the bottom wheel will move anticlockwise, as power output.

Being of lower permeability and lower density, usually, aluminum has been chosen as the material for the wheel of MARS. Lower permeability means that the aluminum plate will bring minimum effect on the interaction between magnets on both wheels. Lower density implies that the plate is lighter; thus, smaller friction is caused between the plate and the central rotor. In the meantime, less energy is lost. Further, lower density means lower cost, which is an important factor in industry. Good malleability of aluminum is a very important factor that has to be taken into consideration. Since the two aluminum plates must be produced in the form of thin disks, good malleability of the material can help to make the plate to be shaped easier.

3.4 Advantages of Contactless Gears

Being a kind of magnetic gear, the contactless gear has several advantages compared to mechanical gears. Firstly, there is an air gap between the two wheels, which means that there is minimum friction between them, which will cause minimum energy loss during rotation. Thus the efficiency of power transmission will increase. Additionally, the noise and vibration caused by contact of the wheels will be reduced, which improves the working environment of MARS. Secondly, the weight of MARS is greatly reduced, by using rare earth permanent magnets, such as NdFeB. Moreover, the friction between the wheel and the central bearing will also decrease. Finally, both manufacture and maintenance cost, due to wear and tear of the materials/gears, will be reduced. Next, the

input and output shaft can be completely isolated and sealed which is a good option in fluid delivery system to avoid leakage. In addition, MARS permits misalignment of magnet poles. The neighboring pairs of magnets will be matched and aligned again when they misalign, as a result of magnetic coupling. Simultaneously, this will work as over load protection. The magnets may happen to slip when overload; at this time, the magnets will align again which make the system avoid damage under malfunction or emergency situation.

Even thorough contactless gears have many advantages compared with traditional mechanical gears, MARS, as contactless still has limitations in several areas. Firstly, the material used in magnetic gears may not be as strong as that in mechanical gear; so they may be subjected to damage of fatigue due to high cyclic load. Moreover, since MARS requires magnetic materials, it has Curie temperature, the temperature at which materials lose their magnetic properties. Hence MARS cannot be used in extreme working conditions such as very high temperatures.

CHAPTER 4

CHARACTERIZATION OF MARS

In this chapter, a MARS prototype has been tested in detail. More importantly, charging studies of rechargeable batteries will be considered. In particular, the temperature changes during the operation of MARS have been monitored by an infrared camera, which will be introduced in particular in the last part of this chapter.

4.1 MARS Prototype

4.1.1 Structure of MARS Prototype

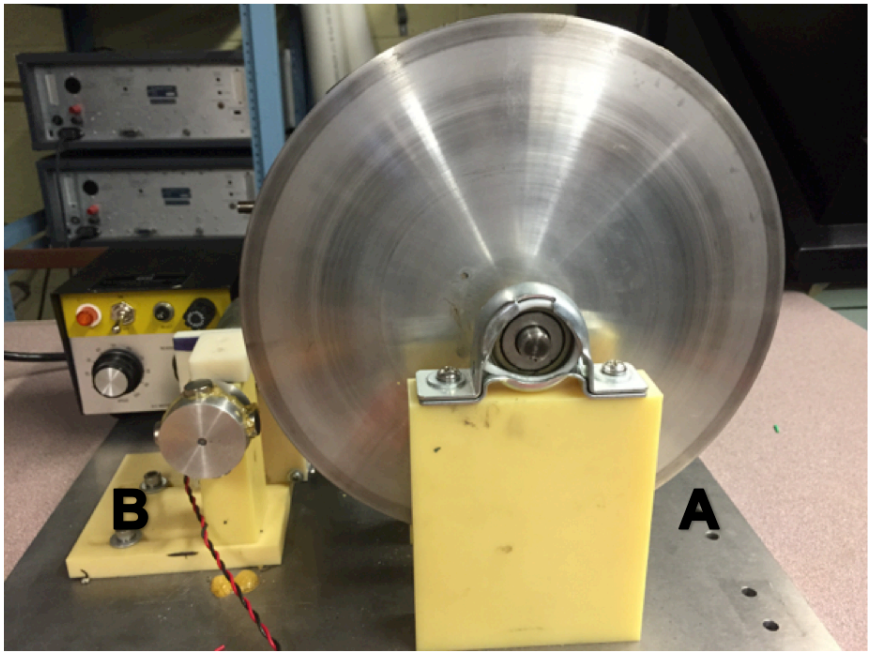

Figure 4.1 MARS prototype.

Figure 4.1 is a picture of a MARS prototype, which is the one we used in our experiments.

This MARS prototype has several advantages. Firstly, the base of MARS is heavier, which makes the system more stable and reduces its resonance. Secondly, a DC electric motor, through which the input power to MARS can be controlled, is connected to the input wheel. Meanwhile, different output power can be obtained by changing the adjustable switch on the power supply to the electric motor. Furthermore, a low-wattage bulb and rechargeable batteries are used to imitate the actual load. The voltage and current are measured in real-time by digital multimeters.

As shown in Figure 4.1, MARS has two wheels, the larger one labeled as Wheel A, and the smaller one labeled as Wheel B. These two wheels have to be in the same plane to make sure that the wheels have the maximum magnetic repelling force. The details of these two wheels are summarized below.

Table 4.1 Parameters of Wheel A

Radius of wheel	11.5 cm
Width of wheel	1.8 cm
Number of magnets on wheel	16

Table 4.2 Parameters of Wheel B

Radius of wheel	3.8 cm
Width of wheel	2.4 cm
Number of magnets on wheel	4

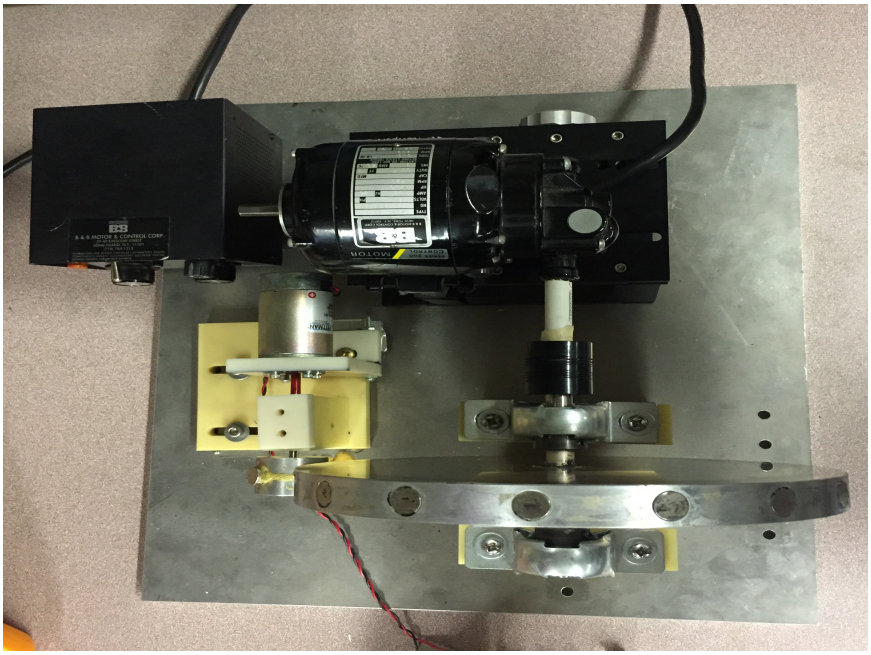

Figure 4.2 Top views of MARS prototype.

Figure 4.2 shows the top view of the MARS prototype. The system has four parts - two magnetic wheels, a DC electric motor and an AC to DC converter. The rotational speed and direction of Wheel A can be changed through the control of motor, thus changing the rotation and direction of Wheel B. The generator, coupled to Wheel B, will collect the output AC power from the wheels and convert it to DC power. This DC electrical power is the total output power of MARS.

4.1.2 Test of MARS

The velocities of the two wheels were monitored by an oscilloscope, as demonstrated in Figure 4.3. This oscilloscope is connected to a magnetic sensor, which is placed very close to Wheel A and can sense and transmit the magnetic field change to the oscilloscope. Every complete wave displayed on the oscilloscope corresponds to the location of a sensor passing a magnet on the wheel. Thus, the velocity of the wheel can

be calculated.

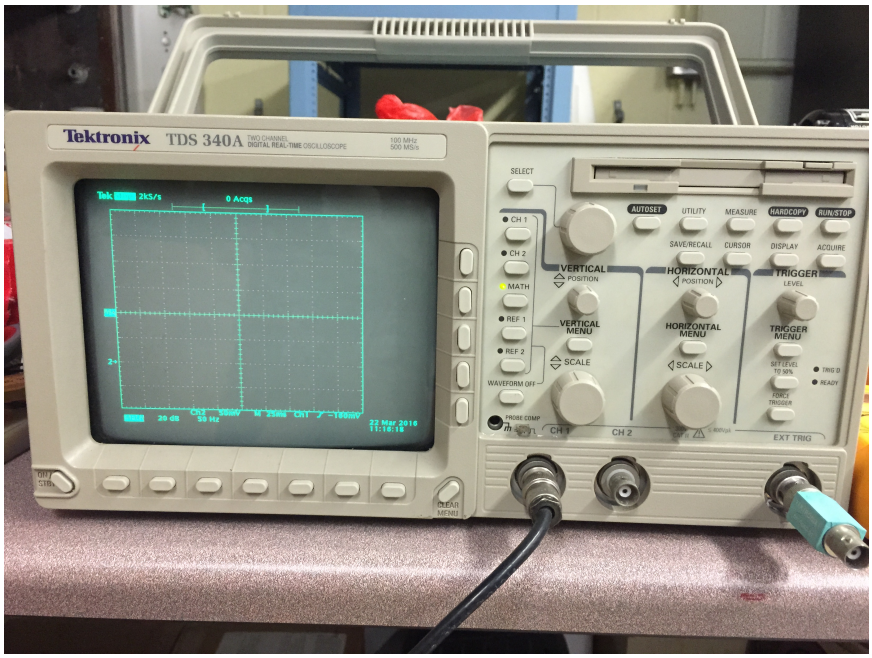

Figure 4.3 Velocity test by magnetic sensor and oscilloscope.

In this way, the velocity of both wheels can be tested. Additionally, different velocities of the two wheels, by changing the input power from the motor, can be tested to confirm if the transfer efficiency of the two wheels is different in higher and lower speed range.

4.2 Integrating Light Bulb

In this section, MARS was used as the power supply to a load in the form of a light bulb. Current and voltage, generated by MARS, was measured using an inline digital ammeter and digital voltmeter, in real-time, in order to know the current and voltage change with changing input power output of MARS.

Figure 4.4 shows the circuit of a light bulb integrated with MARS, in-line digital voltmeter and digital ammeter. A black cable, negative pole, of MARS is connected to the black cable of an ammeter; a red cable from an ammeter is connected to the light bulb; the other input to the light bulb is connected to the red cable of MARS. The voltmeter is connected across the light bulb.

The power input to MARS can be changed by the potentiometer on the power supply. The current and voltage are measured in real-time.

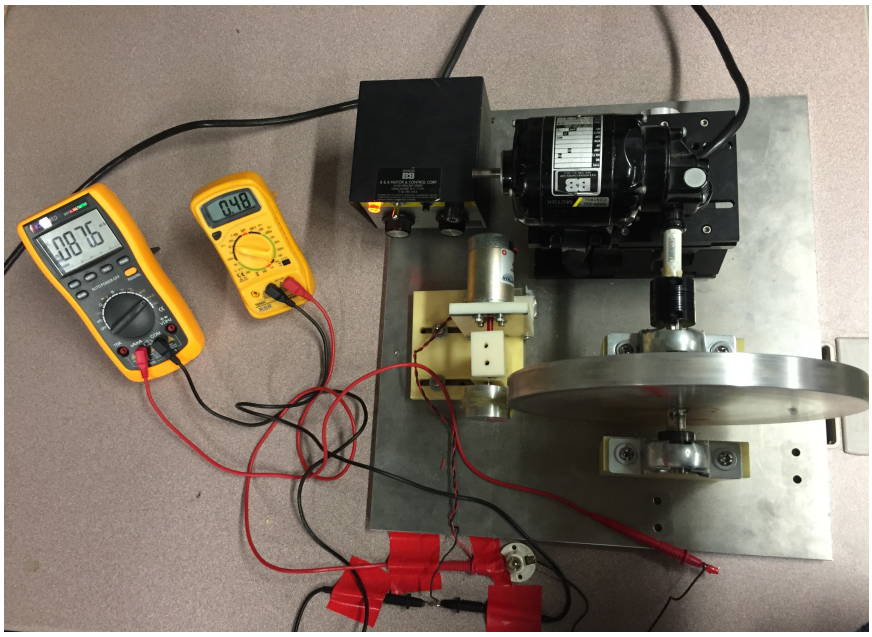

Figure 4.4 Integrating light bulb with MARS.

4.3 Charging the Battery

4.3.1 Structure of the Rechargeable Battery

The structure of the rechargeable battery, which we used in our experiments, is shown in Figure 4.5.

Figure 4.5 Structure of the rechargeable battery.

Source: Panasonic NI-MH handbook http://www.mouser.com/pdfdocs/PanasonicBatteries_NI-MH_Handbook.pdf

In Figure 4.5, 1 is positive pole, 8 is negative pole, 7 is the cathode which is nickel hydroxide, 9 is anode which is a certain hydrogen-absorbing alloy, 2 is the top plate, 10 is the insulation plate, 5 is collector and 6 is separator. 3 is gasket, 4 is safety vent and 11 is exhaust gas hole and 12 is the central tube.

4.3.2 Principle of Electrochemical Reaction Involved in Batteries

Ni-MH batteries employ nickel hydroxide for the positive electrode similar to Ni-Cd batteries. The hydrogen is stored in a hydrogen-absorbing alloy for the negative electrode, and an aqueous solution consists mainly of potassium hydroxide for the electrolyte. Their charge and discharge reactions are shown below [25].

In the charging process,

$$\text{Positive electrode: } Ni[OH]_2 + [OH]^- \xrightarrow{Charge} NiOOH + H_2O + e^- \quad (4.1)$$

$$\text{Negative electrode: } M + H_2O + e^- \xrightarrow{Charge} MH_{ab} + OH^- \quad (4.2)$$

$$\text{Overall reaction: } Ni[OH]_2 + M \xrightarrow{Charge} NiOOH + MH_{ab}\ , \quad (4.3)$$

in which M is hydrogen-absorbing alloy, and $H_{ab}$is absorbed hydrogen.

During the discharging process, the reaction in positive electrode, negative electrode and overall reaction is described below.

$$\text{Positive electrode: } NiOOH + H_2O + e^- \xrightarrow{\text{Discharge}} Ni[OH]_2 + [OH]^- \quad (4.4)$$

$$\text{Negative electrode: } MH_{ab} + OH^- \xrightarrow{\text{Discharge}} M + H_2O + e^- \quad (4.5)$$

$$\text{Overall reaction: } NiOOH + MH_{ab} \xrightarrow{\text{Discharge}} Ni[OH]_2 + M \quad (4.6)$$

As can be seen in the overall reaction above, the main characteristics of the principle behind a Ni-MH battery is that hydrogen moves from the positive to the negative electrode during charging and reverse during discharge. At the same time, the electrolyte does not take part in the reaction, which means there is no accompanying

increase or decrease in the electrolyte. Usually, these reactions take place at the boundary faces of the positive and negative electrodes, respectively.

The hydrogen-absorbing alloy negative electrode can reduce the gaseous oxygen given off from the positive electrode during overcharge successfully by sufficiently increasing the capacity of the negative electrode.

4.3.3 Main Characteristics of the Rechargeable Battery

Usually, the Ni-MH batteries have five main characteristics: charge, discharge, storage life, cycle life and safety [25].

The charge characteristics of Ni-MH batteries are affected by many factors, such as current, time and temperature. For example, the voltage of battery will rise when the charge current is increased or when the temperature is low. Ni-MH batteries should be charged at a temperature ranging from 0°C to 40°C using a constant current of 1C or less. Repeated charge at high or low temperatures causes the battery performance to deteriorate. Furthermore, repeated overcharge should be avoided since it will downgrade the battery performance.

Practically, the discharge characteristics of Ni-MH batteries are affected by many factors, like current and temperature. The discharge voltage characteristics are flat at 1.2V, which is almost the same as for Ni-Cd batteries. The discharge voltage and discharge efficiency will decrease as the current rises or the temperature drops.

The cycle life of these batteries is determined by the conditions under which they are charged and discharged, temperature and other conditions of use. Usually, under proper conditions of use, these batteries can be charged and discharged for more than 500 cycles.

Storage characteristics include two different parts, self-discharge characteristics and restoration characteristics. Self-discharge is affected by the temperature at which the batteries are left standing and the length of time during which they are left standing. It increases in proportion as the temperature or the shelf-standing time increases.

The safety vent on the battery will activate to prevent battery damage when its internal pressure rises due to overcharge, short-circuiting, reverse charge or other conditions.

4.3.4 Charging Studies

The process of charging the rechargeable battery is the same as lighting the light bulb, shown in the figure below. The battery is discharged completely before the experiment.

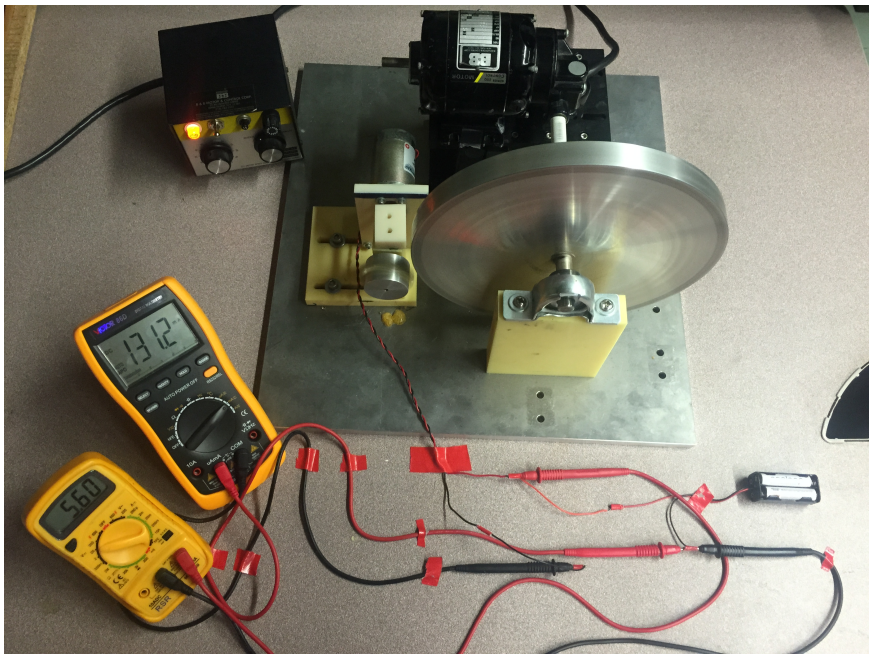

Figure 4.6 Charging the rechargeable battery.

Meanwhile, the voltage and current of the system will be measured every ten minutes during charging. In this way, the change in voltage and current with time will be analyzed. Additionally, the duration to charge the battery completely will be determined.

4.4 Thermal Imaging of MARS

4.4.1 History of Infrared Technology

The discovery of the infrared component of the electromagnetic spectrum was made by William Herschel - the Royal Astronomer to King George III of England [26], in 1800 when he was searching for an optical filter material to reduce the brightness of the sun's image in telescopes during solar observation. When he tested different samples of colored glass that gave similar reductions in brightness, he found that some of these samples permitted lots of sun's heat to pass through while others passed little.

In order to find a material that would give the desired reduction in brightness as well as the maximum reduction in heat, Herschel began an experiment by repeating Newton's prism experiment, but looking for the heating effect rather than the visual distribution of intensity in the spectrum. Initially, he blackened the bulb of a sensitive mercury-in-glass thermometer with ink, and with this as his radiation detector, he proceeded to test the heating effect of the various colors of the spectrum formed on the top of a table by passing sunlight through a glass prism [26]. Other thermometers placed outside the sun's rays served as controls. As a result, he found that the temperature readings showed a steady increase from the violet end to the red end as the color detected by the blackened thermometer changed, which was the same result as the Italian researcher, Landriain [26], in a similar experiment in 1777. More importantly, he found the

point at which the heat reached a maximum, and it was beyond the red end. This point was known as the 'infrared wavelengths'. Also, the new portion of the electromagnetic spectrum was referred as the ' thermometrical spectrum'.

In 1829, the invention of the thermocouple by Nobili [26] changed the approach to thermometry. The Nobili models could be read to temperature accuracies of 0.05℃; however, Herschel's thermometer could be read to temperature accuracies of 0.2℃. Then, Melloni [26], an Italian investigator, did the more essential work; he connected a number of thermocouples in series to form the first thermopile, which improved the sensitivity of the thermometer for detecting heat radiation remarkably. The distance for detecting heat was also improved to three meters away. In addition, the invention of the bolometer by Langley, in 1880, improved the sensitivity of the infrared-detector. This bolometer consisted of a thin blackened strip of platinum connected in one arm of a Wheatstone bridge circuit upon which the infrared radiation was focused and to which a sensitive galvanometer responded [26].

Between the years 1900 and 1920, many patents focused on infrared radiation were issued. These patents were more on devices to detect personnel, artillery, aircraft, and ships. The first operating systems were developed during the 1914-1918 war, when both sides were urging for improvement in the military strength by deployment of infrared systems. At that time, the most sensitive system was based on the variation of the bolometer idea. However, between the two wars, the infrared detectors had two revolutionary developments: the photon detector and the image converter, among which the image converter aroused the greatest attention since it enabled an observer to 'see in the dark' for the first time.

4.4.2 Theory of Thermography

Electromagnetic spectrum is divided into several wavelength regions, called bands. Thermography makes use of the infrared spectral band, which is further divided into four smaller bands [26]: the near infrared (0.75-3μm), the middle infrared (3-6 μm), the far infrared (6-15μm) and the extreme infrared (15-100 μm).

Blackbody is defined as an object which absorbs at emits all electromagnetic radiation. In principle, the blackbody source can be constructed easily. For example, the aperture in an isotherm cavity made of an opaque absorbing material nearly has the same properties with blackbody. This isothermal cavity will generate blackbody radiation when heated to a certain temperature, whose characteristics are only determined by the temperature of the cavity. At this time, the heated isothermal cavity is called cavity radiator, which is used in cameras manufactured by FLIR Systems as sources of radiation for temperature reference standards in the laboratory for calibrating thermographic instruments.

There are three expressions that describe the radiation emitted from a blackbody [25]:

1. Planck's Law
   Planck's law describe the spectral distribution of the radiation from a blackbody; the formula is as follow:

$$W_{\lambda b} = \frac{2\pi hc^2}{\lambda^5\left(e^{hc/\lambda kT}-1\right)} \times 10^{-6}[Watt/m^2, \mu m] \quad (4.1)$$

where:

Table 4.3 Parameters for Planck's Law

$W_{\lambda b}$	Blackbody spectral radiant emittance at wavelength λ
c	Velocity of light=$3\times10^{8}\ m/s$
h	Plank's constant=$6.6\times10^{-34} Joule\ sec.$
k	Boltzmann's constant= $1.4\times10^{-23} Joule/K$
T	Absolute temperature (K) of a blackbody
λ	Wavelength (μm)

2. Wien's displacement law
   Wien's formula shows the relative point of wavelength, in which the color changes from red to orange or yellow with increasing temperature, as described below:

$$\lambda_{max} = \frac{2898}{T}[\mu m] \tag{4.2}$$

3. Stefan-Boltzmann's law

Stefan-Boltzmann formula states that the total emissive power of a blackbody is proportional to the fourth power of its absolute temperature, as represented by the following equation:

$$W_b = \sigma T^4 [Watt/m^2], \tag{4.3}$$

in which W_b is the area below the Planck curve for a particular temperature, T.

4.4.3 Thermal Imaging of MARS

The thermal imaging technology, as introduced in the previous section, offers a possibility to measure the temperature of the charging system integrated with MARS. By taking the thermal image, overheating of components such as batteries/power supplies can be avoided which is very meaningful.

There are several parameters that have to be set up before measuring the temperature: distance between the front lens of infrared camera and object, emissivity of objective, reflected apparent temperature and relative humidity. Emissivity is the most important object parameter, which is used to measure how much radiation is emitted from the object, compared to that from a perfect blackbody at the same temperature. Normally, object materials and surface treatments exhibit emissivity ranging from approximately 0.1-0.95. And as each part of the system has different emissivity, the emissivity of the whole system has to be set as 0.95. Distance was used to compensate for two facts: the atmosphere between the object and the camera absorbs the radiation from the target, and the camera detects that radiation from the atmosphere itself. Additionally, to make sure that the entire charging system can be imaged in the infrared, the distance between the lens of the camera and the charging system was set at 0.6 m. Additionally, since each part of the system has different heights, this difference in height has to be ignored. The light bulb or the rechargeable battery was taken as the reference. The reflected temperature usually was set when the emissivity is low and the objective temperature is relatively far from that of the reflected temperature. In this experiment, the emissivity is high, 0.97; as a result, the reflected apparent temperature is 0. Relative humidity is used to compensate

for the transmittance, which depends on the humidity in the atmosphere. For short distance and normal humidity, relative humidity has a value of 50%.

In order to monitor the changing temperature, thermal image of the charging system is taken every 10 minutes. The camera must remain stationary in these measurements. Additionally, during the capture of different images, the selected measuring point of each part must be the same.

After taking the infrared image and selecting the measurement point, the temperature of each part can be analyzed using the software provided by FLIR. By recording the temperature and plotting a graph of temperature change versus time, the trend in temperature can be clearly seen.

CHAPTER 5

RESULTS AND DISCUSSION

5.1 Transmission Efficiency of MARS

Table 5.1 shows the test result of MARS.

Table 5.1 Test Results of MARS

Number of Experiment	Angular Velocity Wheel A, RPM	Angular Velocity Wheel B, RPM	Ratio of Velocity B/(A*4) %
1	35.18	139.8	99. 33
2	75.42	253.68	84.09
3	102.18	385.48	94.31
4	126.56	482.28	95.26
5	150	580.84	96.81
6	175.92	705.84	100.30
7	200.68	824.96	102.77
8	225.17	866.64	98.44
9	243.33	996.16	102.35
10	263.50	1087.12	103.14

From Table 5.1, as can be seen from the computed ratio of frequency, four times the angular velocity of wheel A (16 magnets) and the angular velocity of wheel B (4 magnets) are very close, which means that the two wheels rotate simultaneously. As a result, the energy loss in transmission between the two wheels is small. The synchronous rotation of the two wheels of MARS also means that all the energy input to wheel A is transmitted to wheel B. Moreover, it shows that the MARS system is efficient.

Additionally, the magnetic field generated by MARS was tested and shown in Table 5.2. The test point is labeled in Figure 5.1.

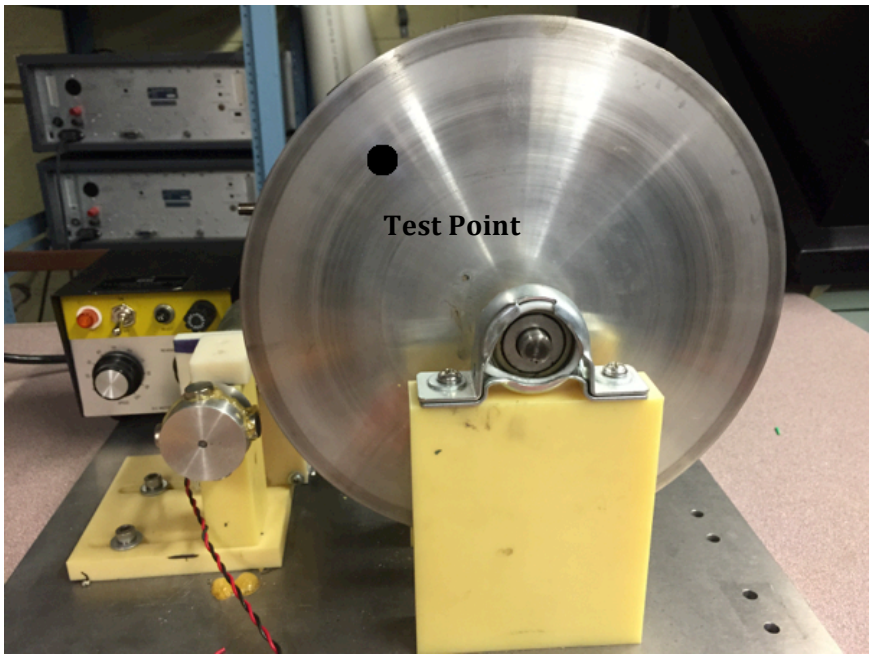

Figure 5.1 Test point of magnetic field intensity.

Table 5.2 Intensity of Magnetic Field for Different Angular Velocity

Angular Velocity/RPM	Intensity of Magnetic Field /mG
75.42	26.93
126.56	105.1
175.92	142.7
225.17	183.2
263.5	219.8

5.2 Voltage and Current of Charging System

5.2.1 Integrating Light Bulb

Following the process shown in Section 4.2.1, a light bulb was used as the load and the corresponding voltage and current were measured, as shown in the Table 5.3.

Table 5.3 Voltage, Current and Power for Different Angular Velocity - Light Bulb

Angular Velocity/RPM	Current/mA	Voltage/V	Power/V
75.42	70.9	0.651	0.046
126.56	133.3	1.031	0.1374
175.92	219.6	1.586	0.3483
225.17	258.7	2.18	0.564
263.5	285.3	2.78	0.7931

According to the data above, the results are shown in Charts 5.1 and 5.2.

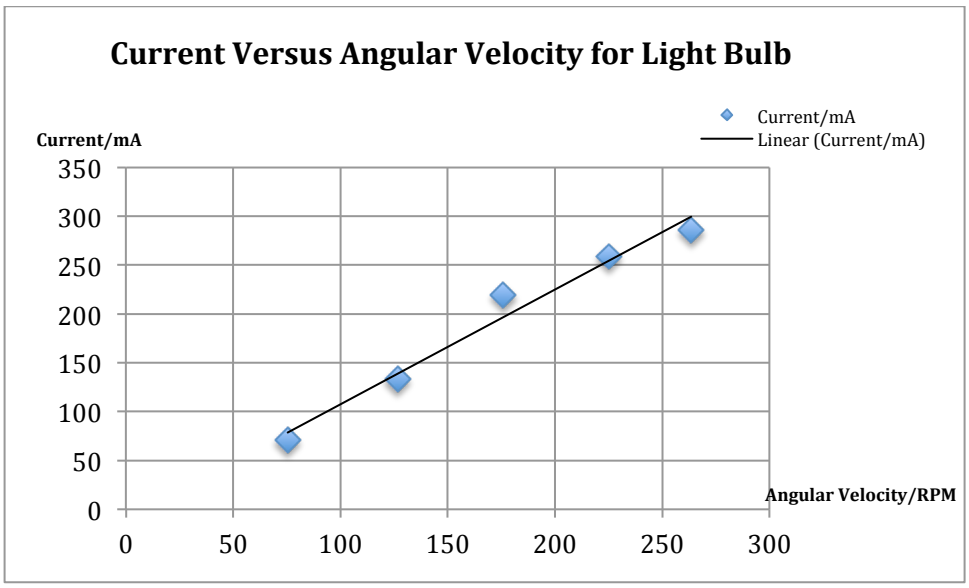

Chart 5.1 Current versus angular velocity for light bulb.

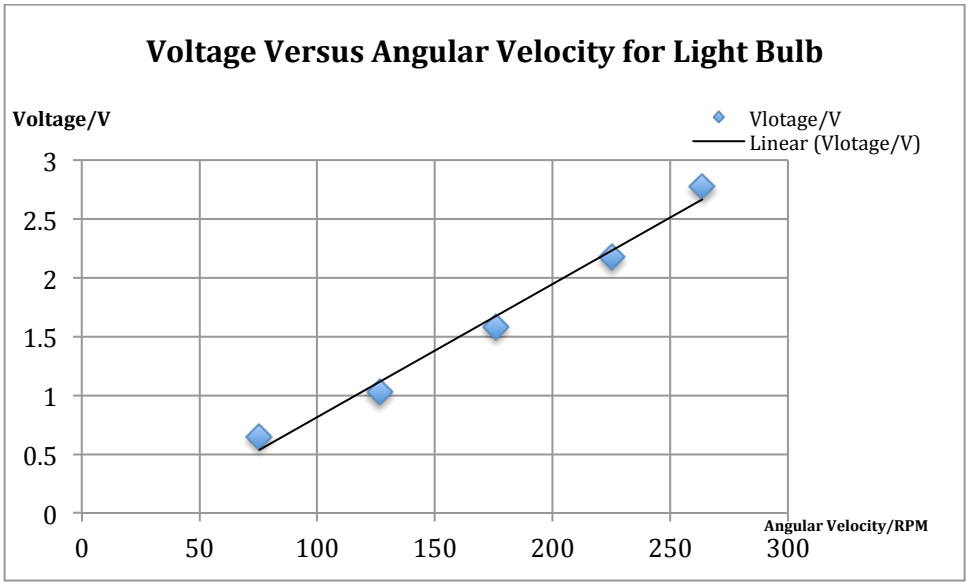

Chart 5.2 Voltages versus angular velocity for light bulb.

Table 5.3 shows the variations in current and voltage for different angular velocity, and the power is increased. As the angular velocity increases, the current and voltage are increased, which contribute to the power increase from 0.046W to 0.7931W. Moreover, in Charts 5.1 and 5.2, the increase in current and voltage are stable.

5.2.2 Charging the Rechargeable Battery

The battery used in our experiment is Eneloop^{TM}, made by Panasonic, model number is BK-4MCCA, AAA. For each battery, its rated voltage is 1.5V, and its capacity is 750mAh. In our experiment, four rechargeable batteries were used, in order that the total voltage of batteries is close to the maximum output voltage of MARS.

As illustrated in Section 4.4.2, the voltage changes depend on the charging time that was measured and recorded in Table 5.3. The chart was drawn based on Table 5.4, and shown in Chart 5.3.

Table 5.4 Voltage Changes Versus Charging Time

Time of charging Minutes	**Voltage V**
0	4.5
5	5.4
10	5.47
15	5.51
20	5.52
25	5.54
30	5.55
35	5.56
40	5.56

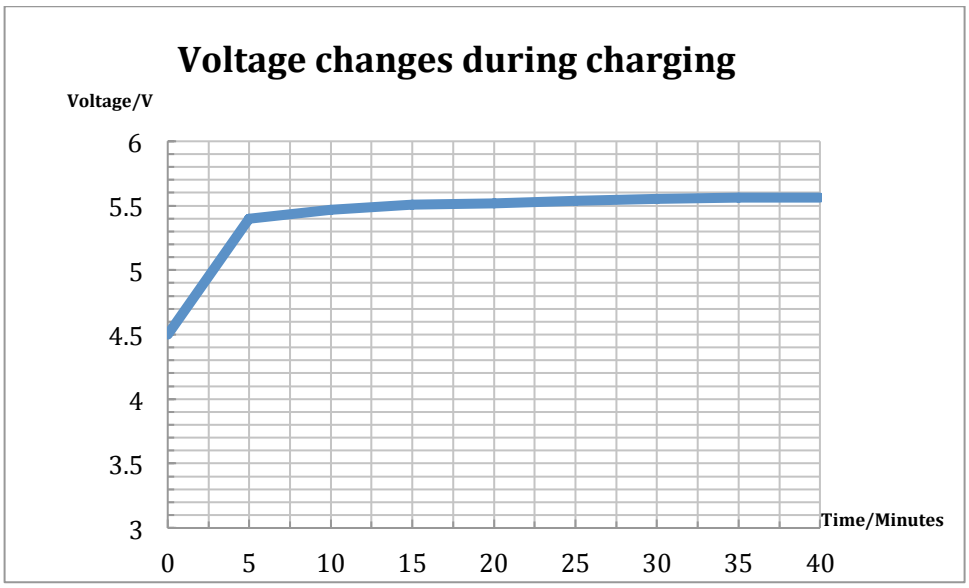

Chart 5.3 Voltage changes during charging.

In Table 5.3 and Chart 5.3, the initial voltages of the batteries are 4.5V, 1.125V for each battery, which means that the batteries are basically fully discharged. The batteries are charged most rapidly, most efficiently in the first 5 minutes, charging from 4.5V to 5.4V. After 10 minutes, the voltage increases relatively slowly and finally reaches 6V.

In this charging system, the rotation velocity of MARS Wheel A is 450RPM. Thus the power generated by MARS, under 450RPM, can charge the electrical equipment with rated voltage of about 6V. Suppose MARS has higher rotation velocity, it will generate more power, which leads to wider application. At the same time, the wheel of MARS may connect to the windmill; the rotation of windmill, due to wind, will make the wheel of MARS to rotate, thus the power is generated. This is a great way to generate energy without pollution.

The current changes during charging are illustrated in Tables 5.5 and 5.6.

Table 5.5 Current Changes Versus Charging Time

Time of charging Minutes	Current mA	Time of charging Minutes	Current mA
0	144.2	10	128.1
0.5	115.9	10.5	118.9
1	109.4	11	121.2
1.5	109.3	11.5	125.7
2	114.5	12	127.3
2.5	115.2	12.5	120.8
3	111.5	13	122.8
3.5	116.6	13.5	125.2
4	114.2	14	124.3
4.5	114.5	14.5	121.1
5	118	15	122.3
5.5	114.1	15.5	121.4
6	124.1	16	116.3
6.5	124.4	16.5	116.7
7	126.3	17	117.9
7.5	116	17.5	124.5
8	116.9	18	115.7
8.5	123.3	18.5	121.5
9	123.3	19	124.9
9.5	123.9	19.5	113.5

Table 5.6 Current Changes Versus Charging Time (Continued)

Time of charging Minutes	Current mA	Time of charging Minutes	Current mA
20	117.2	30	125.5
20.5	120.7	30.5	129.1
21	122.1	31	119.6
21.5	124.9	31.5	116.1
22	119.8	32	127.3
22.5	119.8	32.5	123.6
23	124.1	33	116.1
23.5	122.2	33.5	116.9
24	122.2	34	123.3
24.5	119.7	34.5	122.6
25	114.5	35	123.7
25.5	127.6	35.5	133.7
26	124.3	36	131.6
26.5	124.9	36.5	127.3
27	123.4	37	127.8
27.5	129.5	37.5	127.2
28	125.1	38	130.9
28.5	135.6	38.5	127
29	133.3	39	133.4
29.5	126.9	39.5	124.2

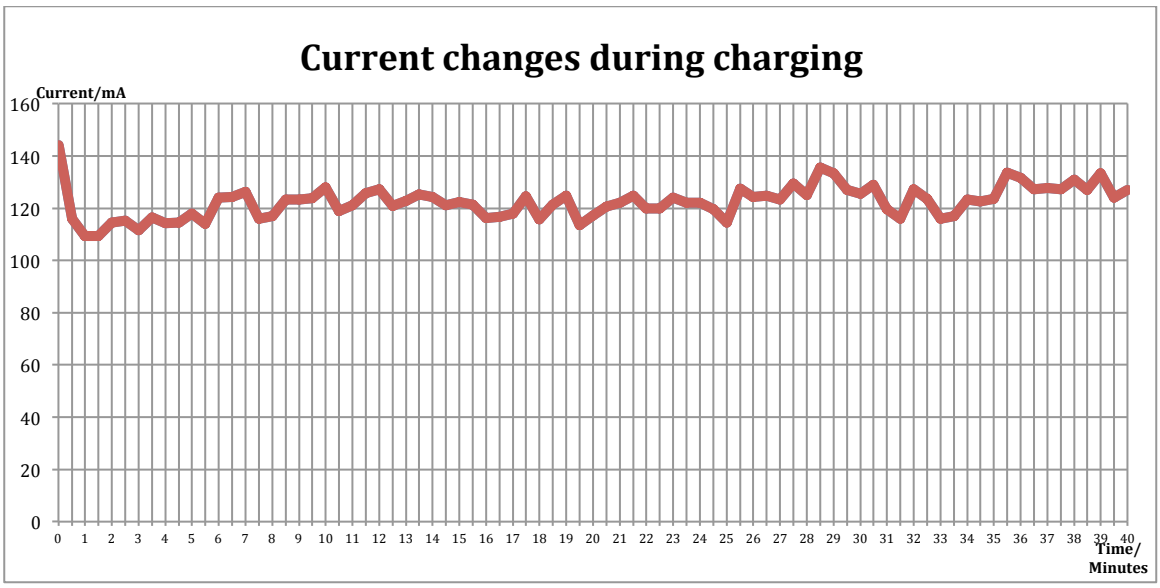

Chart 5.4 Current changes during charging.

From Tables 5.5 and 5.6, Chart 5.4, the current during charging is relatively stable, around 120mA. This testing result means that the whole charging process is stable in current, which is very critical for the batteries.

To further explore how the current and voltage changes in the first 6 minutes during charging, another charging experiment was done. The results are shown in Table 5.7 and Chart 5.5.

Table 5.7 Voltage Changes During the First 6 Minutes

Time of charging Minutes	Volt V
0	4.28
1	5.2
2	5.33
3	5.41
4	5.44
5	5.47
6	5.48

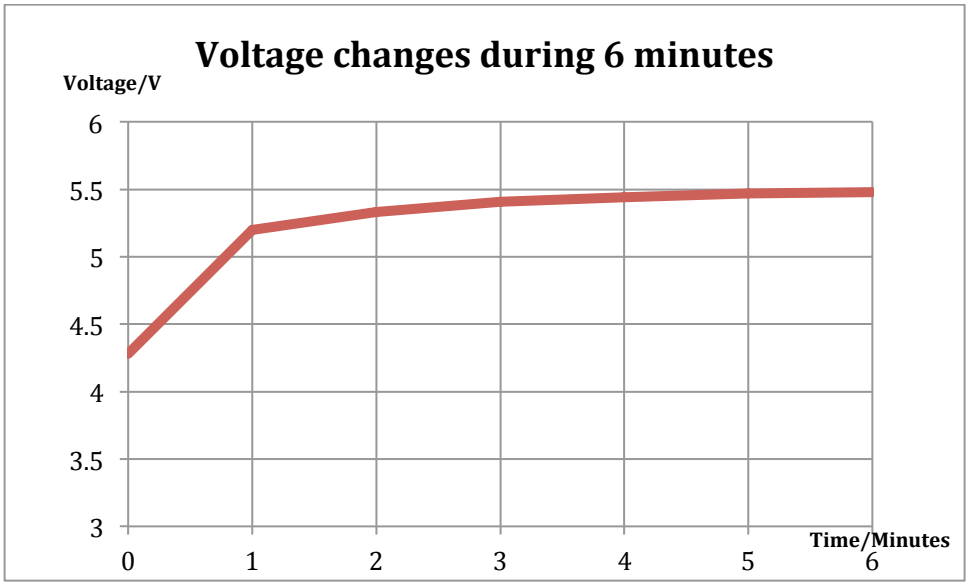

Chart 5.5 Voltage changes during charging.

In this experiment, the initial voltage of the batteries is 4.28V. From the data in Table 5.7, the charging process is the most efficient in the first 5 minutes, the batteries were charged from 4.28V to 5.47V. The current during these measurments are shown in the Table 5.8 and Chart 5.6.

Table 5.8 Current Changes During the First 6 Minutes

Time of charging Minutes	Current mA	Time of charging Minutes	Current mA
0	107.1	3.5	126.3
0.5	122.9	4	126.9
1	107.3	4.5	128.9
1.5	120	5	128
2	120.8	5.5	119.2
2.5	125.8	6	119.5
3	111.6		

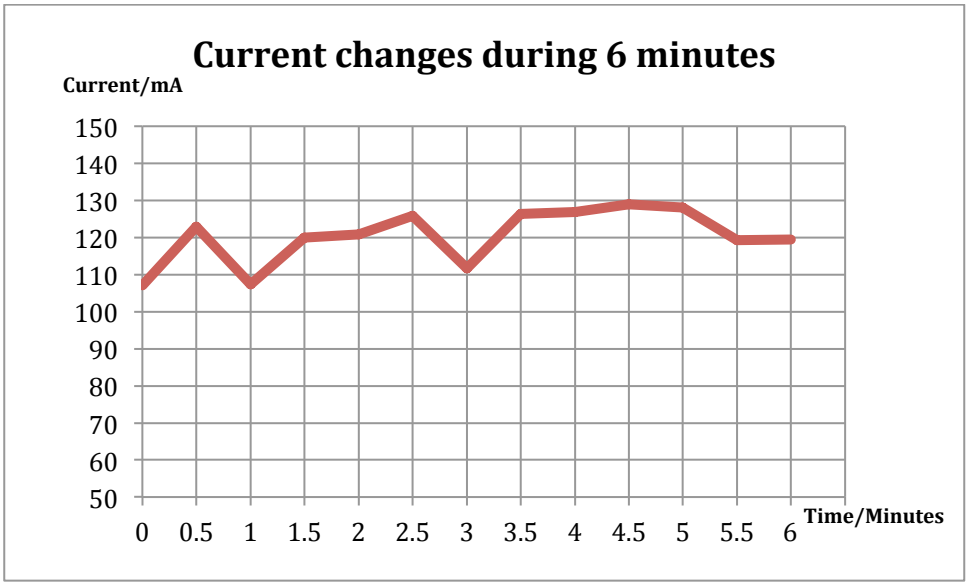

Chart 5.6 Current changes during 6 minutes.

The current in the first 6 minutes is stable around 120mA. The charging current is always stable, which makes MARS a more safe and useable system.

To make the output voltage of MARS stable, a transformer was added to the system, as shown in the Figure 5.2. Additionally, the voltage and current during charging

of the new system were measured and shown in Table 5.9. At the same time, the testing result of MARS charging system was shown in the same chart, which helps to better analyze the properties of the new system.

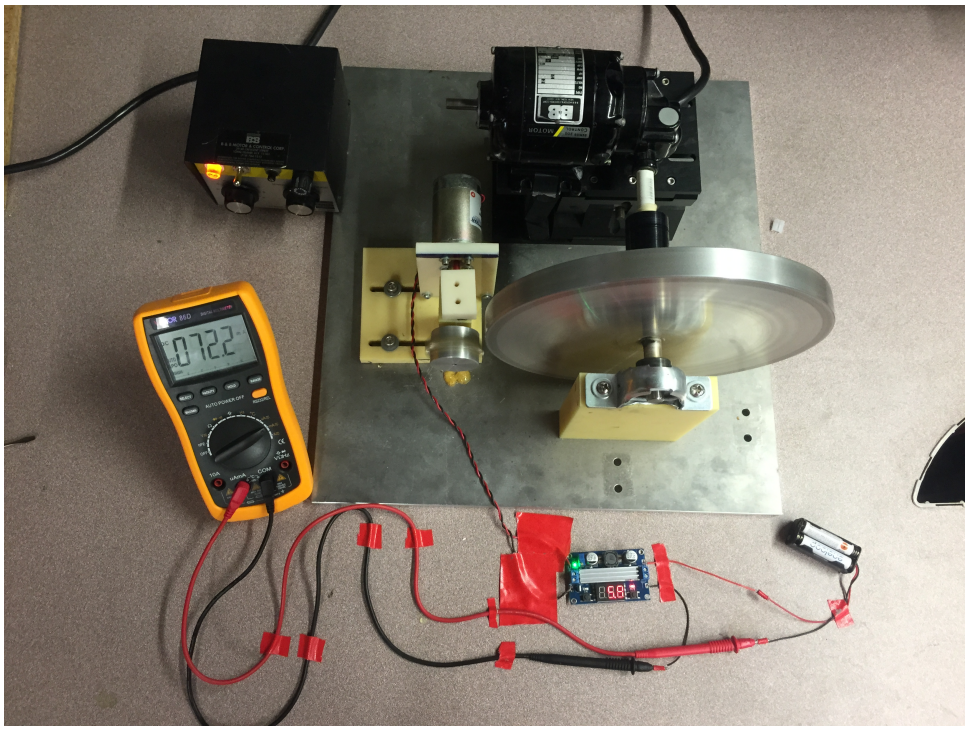

Figure 5.2 Modifications of MARS.

Table 5.9 Current Changes During 6 Minutes After Adding Transformer

Time of charging Minutes	Current mA	Time of charging Minutes	Current mA
0	96	3.5	87.2
0.5	81	4	98.2
1	81.7	4.5	95
1.5	75.5	5	93.5
2	90.9	5.5	85.2
2.5	84	6	89.2
3	88.5		

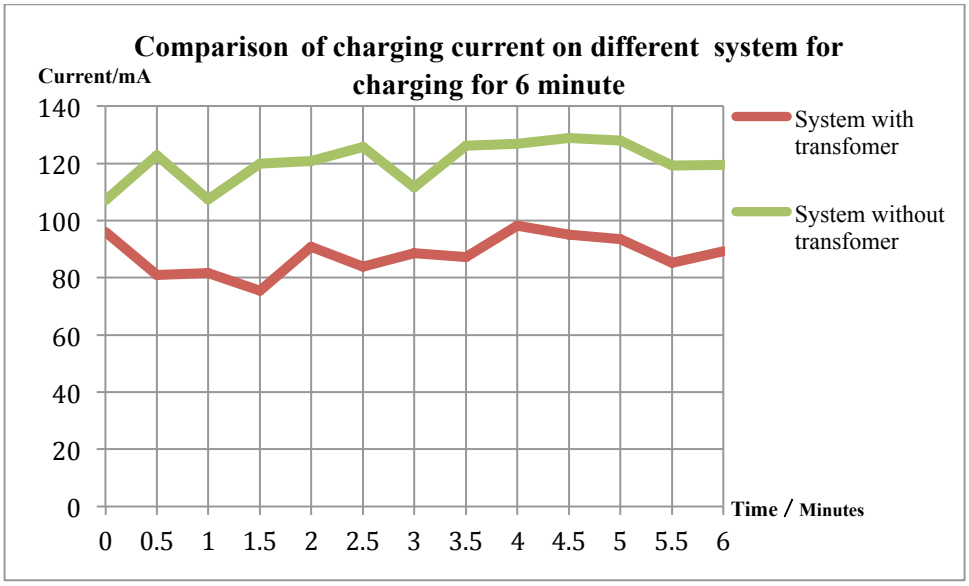

Chart 5.7 Comparison of charging current on different system for charging for 6 minutes.

Table 5.10 Voltage Changes During 6 Minutes After Adding Transformer

Time of charging Minutes	**Volt V**
0	4.774
1	5.284
2	5.366
3	5.389
4	5.392
5	5.419
6	5.422

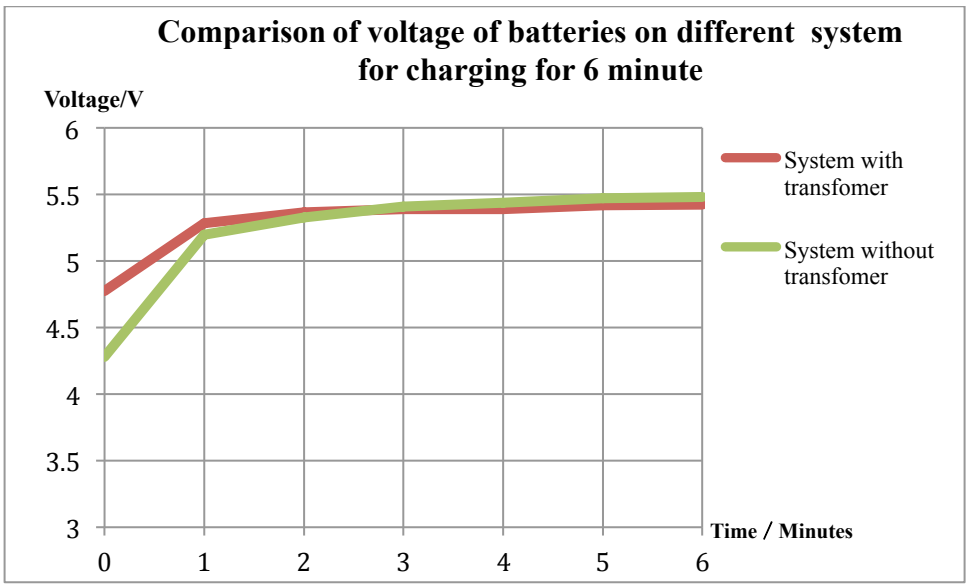

Chart 5.8 Comparison of voltage of batteries on different system for charging for 6 minutes.

The charging voltage is 6V after using the transformer.

By adding the transformer to the output power generated by MARS, the stability of the charging system was improved; at the same time, the charging efficiency relatively decreased within 6 minutes. In Table 5.10, the voltage of the batteries increased from 4.47V to 5.42V in 6 minutes, which is smaller compared to the charging system without transformer. At the same time, compared to the system without the transformer, the charging current of the new charging system was reduced, as a result of increasing the charging voltage by the transformer. Since the total charging power is constant, increasing the charging voltage will decrease the charging current, from average 120mA to 88mA.

Table 5.11 Voltage Changes Versus Charging Time After Adding Transformer

Time of charging Minutes	Volt V
0	4.774
5	5.419
10	5.449
15	5.468
20	5.476
25	5.488
30	5.502
35	5.507
40	5.519

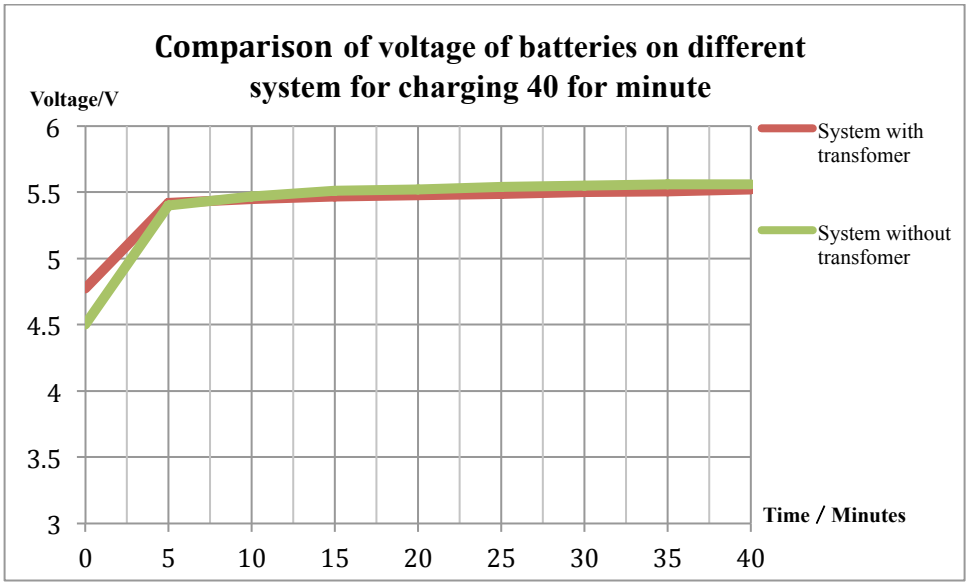

Chart 5.9 Comparison of voltage of batteries on different system for charging for 40 minutes.

Table 5.12 Current Changes Versus Charging Time After Adding Transformer

Time of charging Minutes	Current mA	Time of charging Minutes	Current mA
0	96	10	97.6
0.5	81	10.5	102.9
1	81.7	11	99.3
1.5	75.5	11.5	99.4
2	90.9	12	101.7
2.5	84	12.5	101.2
3	88.5	13	98
3.5	87.2	13.5	100.9
4	98.2	14	104.3
4.5	95	14.5	103.6
5	93.5	15	103.8
5.5	85.2	15.5	100.8
6	89.2	16	98.5
6.5	102.5	16.5	96.7
7	98.8	17	95.3
7.5	97.2	17.5	95.5
8	95.3	18	97.4
8.5	98.9	18.5	94.6
9	99.4	19	93.8
9.5	100.3	19.5	96.6

Table 5.13 Current Changes Versus Charging Time After Adding Transformer (Continued)

Time of charging Minutes	Current mA	Time of charging Minutes	Current mA
20	99	30	99.4
20.5	100.9	30.5	98.4
21	107.8	31	97.7
21.5	99.6	31.5	98.7
22	101.9	32	97.6
22.5	102.7	32.5	98.7
23	100.3	33	97.7
23.5	98.1	33.5	93.7
24	101.3	34	94.4
24.5	96.8	34.5	94.9
25	96.8	35	99
25.5	96.7	35.5	101.3
26	94	36	101.5
26.5	95	36.5	99.7
27	102.3	37	95.9
27.5	105.1	37.5	98.4
28	103.4	38	101.8
28.5	102.4	38.5	100.8
29	100.7	39	103.2
29.5	100	39.5	103.4

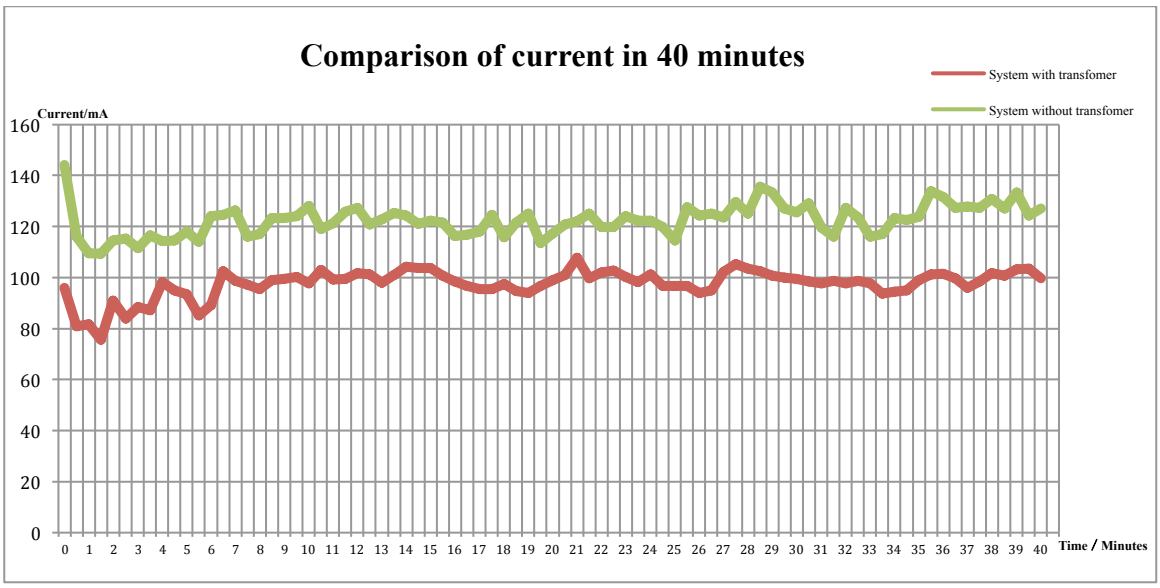

Chart 5.10 Comparison of current in 40 minutes.

In Charts 5.9 and 5.10, the charging current on the batteries in the MARS system with transformer is relatively small compared to the MARS system without transformer; after charging for 40 minutes, the total increase in batteries' voltage in the system without transformer is greater than that in the system with transformer. The standard deviation, which is used to quantify the amount of variation or dispersion of data, was calculated based on the two sets of data: the standard deviation for the system with transformer is 5.60 and for the system without transformer is 6.15. This means that the current in the system with transformer is more stable. So adding the transformer to the charging system decreases the total charging efficiency, but also makes the charging current and voltage stable. In this way, the MARS charging system overcomes one of the major challenges, unstable output power as a result of periodic magnetic force between magnets of the two wheels, and it has more potential in practice.

Moreover, to explore that if the MARS can charge batteries with higher rated voltage, the 12 volts rechargeable battery is charged, as in Figure 5.3. The details about

the battery are listed in the Table 5.14. The output power of MARS can be amplified to 11.5V by using the transformer.

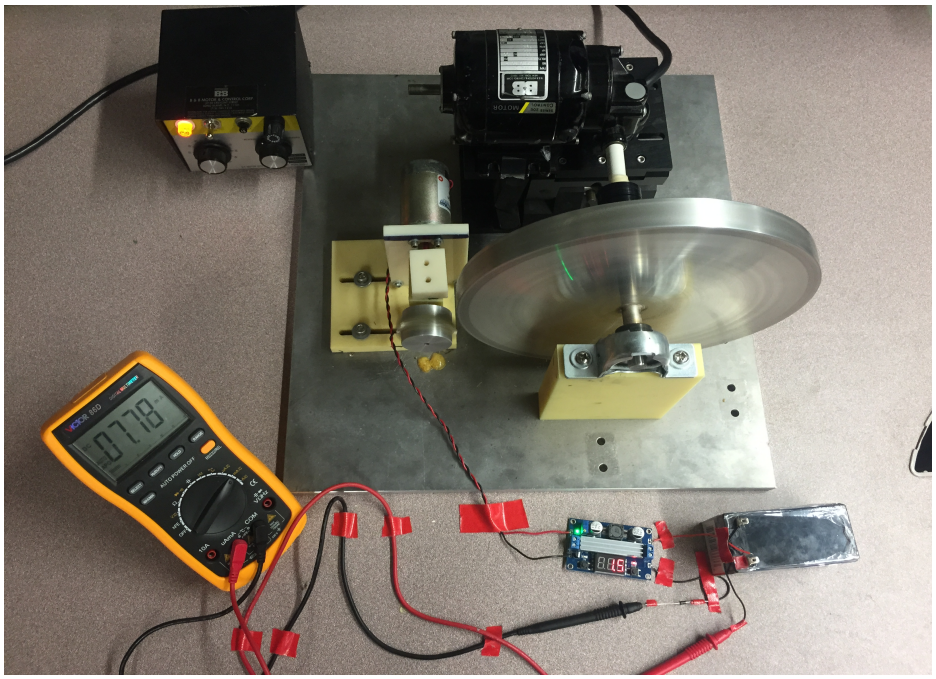

Figure 5.3 Charging 12V rechargeable battery.

Table 5.14 Details of 12V Rechargeable Battery

Brand	ExpertPower
Model	EXP1270
Item Weight	3.2 pounds
Product Dimensions	5.9 x 2.5 x 3.7 inches
Origin	China
Item model number	EXP1270
Manufacturer Part Number	EXP1270
Amperage	7 A
Voltage	12 volts

The current and voltage changes during charging have also been monitored via the ammeter and voltmeter, separately. Testing results are presented in Tables 5.15, 5.16, 5.17, Charts 5.11 and 5.12.

Table 5.15 Voltage Changes During Charging 12V Battery

Time of charging Minutes	**Volt V**
0	9.72
5	10.5
10	10.56
15	10.61
20	10.63
25	10.65
30	10.67

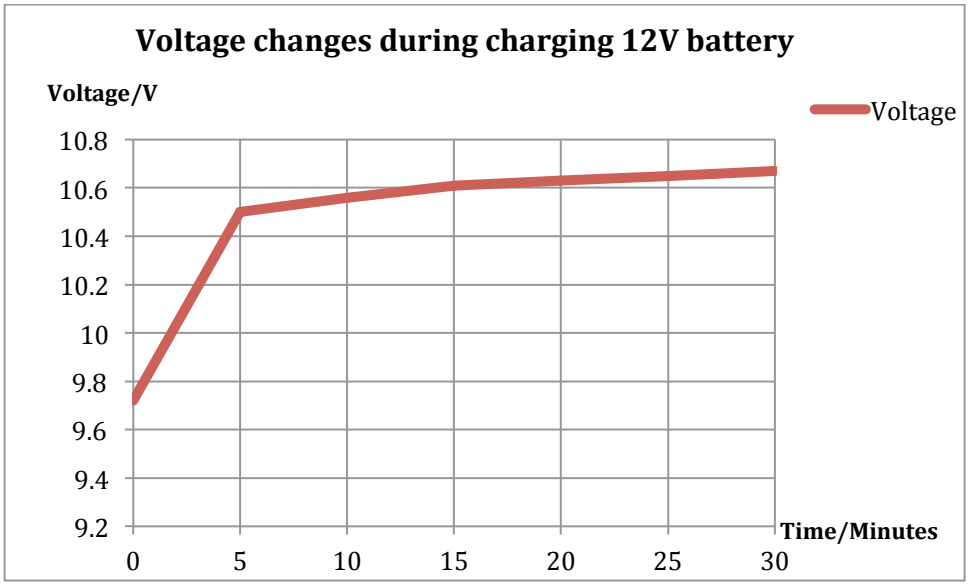

Chart 5.11 Voltage changes during charging 12V battery.

In Chart 5.11, voltage of the battery increases most rapidly within 5 minutes, from 9.72V to 10.5V. From 5 minutes to 30 minutes, the voltage increase is stable, and reaches 10.67V after charging for 30 minutes.

Table 5.16 Current Changes During Charging 12V Battery

Time of charging Minutes	**Current mA**	**Time of charging Minutes**	**Current mA**
0	10.98	8.5	9.12
0.5	10.98	9	9.05
1	10.94	9.5	100.3
1.5	10.93	10	9.13
2	10.81	10.5	8.88
2.5	10.7	11	8.6
3	10.49	11.5	8.57
3.5	10.35	12	8.42
4	10.25	12.5	8.34
4.5	10.09	13	8.26
5	10.63	13.5	8.22
5.5	10.25	14	8.21
6	9.98	14.5	8.08
6.5	9.64	15	8.73
7	9.43	15.5	8.07
7.5	9.3	16	8.05
8	9.2	16.5	7.93

Table 5.17 Current Changes During Charging 12V Battery (Continued)

Time of charging Minutes	Current mA	Time of charging Minutes	Current mA
17	7.85	24	7.37
17.5	7.78	24.5	7.32
18	7.73	25	7.27
18.5	7.67	25.5	7.76
19	7.63	26	7.62
19.5	7.57	26.5	7.54
20	7.53	27	7.44
20.5	7.9	27.5	7.35
21	7.76	28	7.28
21.5	7.7	28.5	7.22
22	7.61	29	7.19
22.5	7.53	29.5	7.15
23	7.48	30	7.76
23.5	7.43		

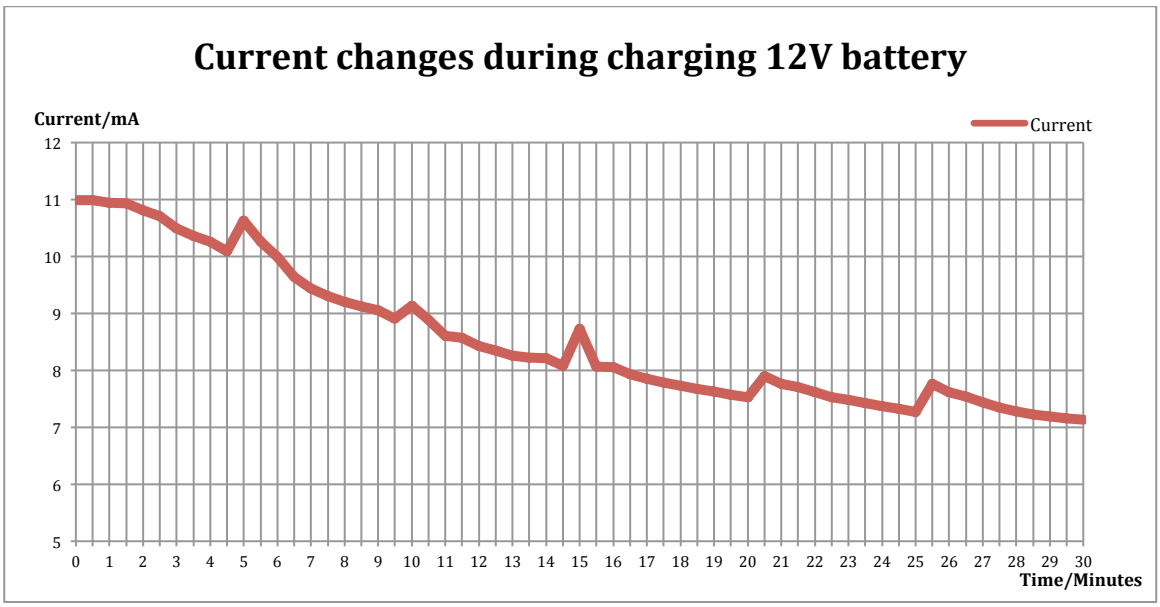

Chart 5.12 Current changes during charging 12V battery.

In contrast to the tendency of current changes during charging 6V rechargeable batteries, the current changes during charging 12V rechargeable battery is different; the current changes during charging 6V batteries is stable, however, it decreases during charging 12V battery. Actually, the current in the system during charging is partially determined by the difference of voltage between the output power of MARS and the voltage of the battery. The output power of MARS is high compared to the 6V batteries, and can keep the current stable even though the voltage of the batteries increase; for the 12V battery, the output power of MARS is not enough to control the current, which makes the current decrease when the voltage of battery decreases. Commonly, charging the 12V rechargeable battery needs more time.

5.3 Thermal Image of Charging System

The thermal image of the charging system was acquired by the infrared camera. The camera model is E6, by FLIR®. Since the emissivity of various part on the charging system is not uniform, the effective emissivity of the system is chosen as 0.97. The images are taken for different charging times, and are shown in the Figures 5.4-5.8.

In the experiment, three measurement points were chosen: Sp1, Sp2 and Sp3, in which Sp1 is a point on the batteries, Sp2 is a point on the wheel of MARS, and Sp3 is a point on the axis of MARS.

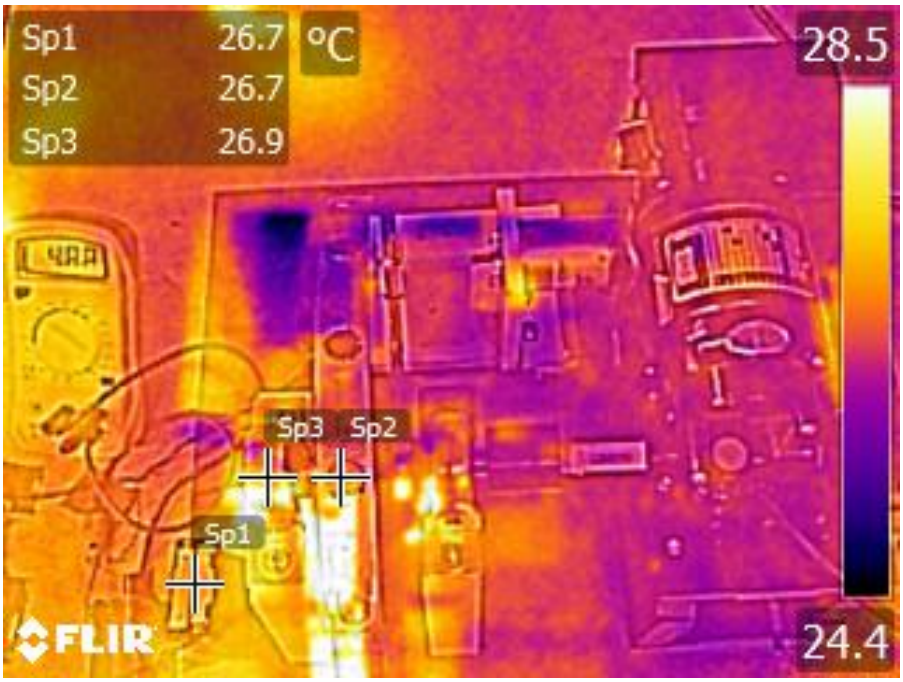

Figure 5.4 Thermal image of the charging system before charging.

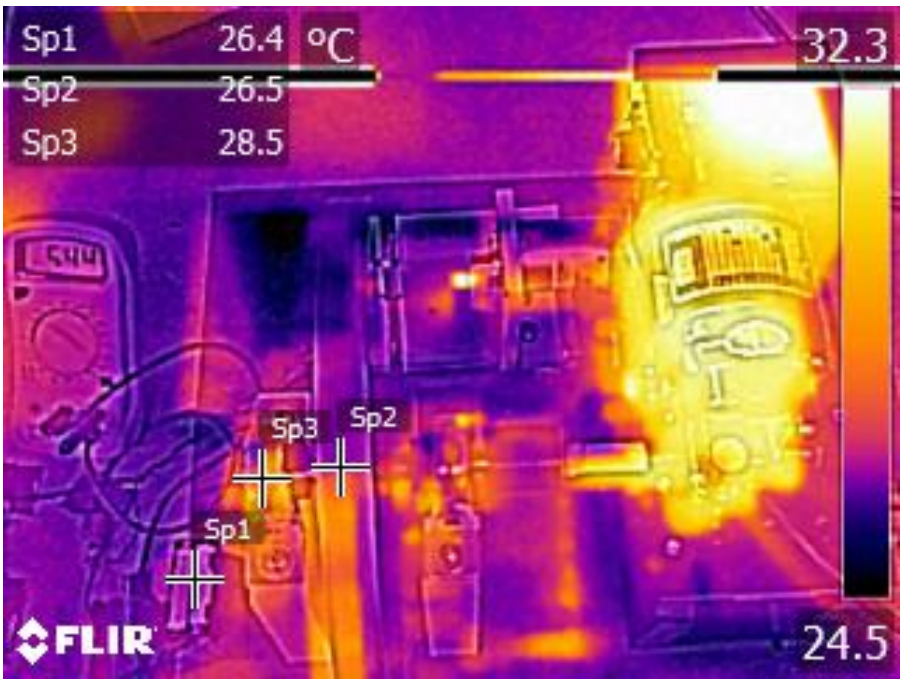

Figure 5.5 Thermal image of the charging system for charging for 10 minutes.

Figure 5.6 Thermal image of the charging system for charging for 20 minutes.

Figure 5.7 Thermal image of the charging system for charging for 30 minutes.

Figure 5.8 Thermal image of the charging system for charging for 40 minutes.

The temperatures of various measurement point are listed in Table 5.18.

Table 5.18 Spatial and Temporal Temperature Distribution

Time	Temperature of Sp1	Temperature of Sp2	Temperature of Sp3
0 minute	26.7℃	26.7℃	26.9℃
10 minutes	26.4℃	26.5℃	28.5℃
20 minutes	28.1℃	28.3℃	30.1℃
30 minutes	28.3℃	28.7℃	30.5℃
40 minutes	30.0℃	30.4℃	35.2℃

For Sp1, the temperature changes from 26.7 ℃ to 30℃ within 40 minutes. This temperature changes were caused by the reaction within the batteries during charging. Actually, the variation in temperature of 3.3℃ is reasonable and does not cause damage to the batteries.

For Sp2, the temperature changes from 26.7℃ to 30.4℃ within 40 minutes. This variation was caused by the rotation of the wheel.

For Sp3, the temperature changes from 26.9℃ to 35.2℃ within 40 minutes. This temperature is very important, because this is the heat caused by the friction between the axis and the fixing device. Local overheating of Sp3 may cause energy loss and even damage the MARS system. Usually, lubrication can decrease the friction. Compared to Sp1 and Sp2, the changing of temperature for Sp3, 7.3℃, is higher than 3.3℃ and 3.7℃, respectively. This means that heating caused by friction on the axis is higher than the heating caused by the reaction within the batteries and wheel. However, the temperature

in Sp3 will not damage the charging system in our experiment. Actually, the heat generated by friction will be one of the problems that should be avoided in further research and development of MARS.

CHAPTER 6

CONCLUSIONS

The energy loss in MARS during transmission between the wheels is relatively small that it can be ignored. In the charging system, depending on MARS, the current gradually increases with voltage, which can reach 3 volts and turn on the light bulb. The energy generated through the MARS system, under the wheel angular velocity of 450RPM, can charge four AAA rechargeable batteries from 4.5V to 5.56V within 40 minutes. Additionally, the batteries can be charged from 4.28V to 5.47V within 6 minutes. The temperature changes in MARS charging system increase by 3.7℃ after charging for 40 minutes.

There are still some weaknesses in the experiment. Firstly, more power will be generated by the MARS system if the angular velocity of wheels was increased. By increasing its angular velocity, the rechargeable batteries with higher rated voltage will be charged, which helps to further test the properties and analyze utilization of MARS. Secondly, the ammeter and voltmeter data were manually acquired which makes the test results less precise. Thirdly, the energy consumed by cables, ammeter and voltmeter are not calculated in the experiment; this may influence the accuracy of test results.

MARS offers a promising approach to generate clean energy. Further development of MARS will lead to wider applications and brighter prospects.

REFERENCES

[1] Magnetism - History Of Magnetism, Retrieved from http://science.jrank.org/pages/4081/Magnetism-History-magnetism.html

[2] I. R. Harris and A. J. Williams, Magnetic Materials, Materials Science and Engineering, Birmingham, UK.

[3] R. Merzouki, A. K. Samantaray, P. M. Pathak, B. Ould Bouamama(2012) Intelligent Mechatronic Systems: Modeling, Control and Diagnosis. Springer, London, UK, p403-405.

[4] C. Carter, Barry, M. G. Norton (2007). Ceramic Materials: Science and Engineering. Springer. pp. 212–15. ISBN 0-387-46270-8.

[5] A. Okamoto(2009) The Invention of Ferrites and Their Contribution to the Miniaturization of Radios, 2009 IEEE Globecom ISBN 978-1-4244-5626-0.

[6] A. H. Neuland(1916) Apparatus for Transmitting Power. US Patent 1171351 A.

[7] H. T. Faus(1941) Magnet Gearing. US Patent 2243555 A.

[8] J. Fraden(2010) Handbook of Modern Sensors: Physics, Designs, and Applications

[9] M. H. Nagrial, J. Rizk(2000) Proceedings of the IEEE International Magnetics Conference.

[10] J. Rizk, M. H. Nagrial, A. Hellany(2004) Proceedings of the 4th International Power Electronics and Motion Control Conference.

[11] M. H. Nagrial, J. Rizk, A. Hellany(2007) Proceedings of the International Conference on Electrical Engineering.

[12] K. Tsurumoto(1989) Some considerations on the improvement of performance characteristics of magnetic gear, IEEE Translation J.

[13] K. Ikuta, S. Makita, S. Arimoto(1991) Non-contact magnetic gear for micro transmission mechanism, in: Proceedings of the Micro Electro Mechanical Systems, An Investigation of Micro Structures, Sensors, Actuators, Machines and Robots, Nara, Japan, pp. 125–130.

[14] S. Kikuchi, K. Tsurumoto(1993) Design and characteristics of a new magnetic worm gear using permanent magnet, IEEE Trans.

[15] W. J. Mabe Jr.(1991) Magnetic transmission, U.S. Patent No. 5,013,949.

[16] Y. D. Yao, D. R. Huang, S. M. Lin, S. J. Wang(1996) Theoretical computations of the magnetic coupling between magnetic gears, IEEE Trans.

[17] Y. D. Yao, D .R. Huang, C. C. Hsieh, D. Y. Chiang, S. J. Wang(1997) Simulation study of the magnetic coupling between radial magnetic gears, IEEE Trans.

[18] D. J. Evans, Z. Q. Zhu(2011) Optimal torque matching of a magnetic gear within a permanent magnet machine, in: Proceedings of the 2011 IEEE International Electric Machines & Drives Conference, ON, Canada, pp .995–1000.

[19] M. Okano, K. Tsurumoto, S. Togo, N. Tamada, S. Fuchino(2002) Characteristics of the magnetic gear using a bulk high-Tc superconductor, IEEE Trans. Appl. Supercond.

[20] K. Atallah, D. Howe(2001) A novel high-performance magnetic gear, IEEE Transactions on Magnetics.

[21] K. Atallah, S. D. Calverley, and D. Howe(2004) Design, analysis and realization of a high-performance magnetic gear,IEE Proc. — Electr.

[22] Y Wu, B Jian(2013), Magnetic field analysis of a coaxial magnetic gear mechanism by two-dimensional equivalent magnetic circuit network method and finite-element method, International Applied Science and Precision Engineering Conference

[23] C Ho, T Chow(2002), Magnetically Augmented Rotation System, U.S. Patent 6356000

[24] N. M. Ravindra(2015) Intelligent Manipulation of Controllable Magnetic Fields Concept to Realization, The International Conference on Materials Science SCI Indexing ,Shanghai, China

[25] Panasonic NI-MH handbook, Retrieved from http://www.mouser.com/pdfdocs/PanasonicBatteries_NI-MH_Handbook.pdf

[26] User's manual Flir Ex series(2013), US